NATIONAL ADVISORY COMMITTEE FOR AERONAUTICS

TECHNICAL NOTE 4170

A REEXAMINATION OF THE USE OF SIMPLE CONCEPTS FOR PREDICTING THE SHAPE AND LOCATION OF DETACHED SHOCK WAVES

By Eugene S. Love

Langley Aeronautical Laboratory
Langley Field, Va.

Washington
December 1957

NATIONAL ADVISORY COMMITTEE FOR AERONAUTICS

TECHNICAL NOTE 4170

A REEXAMINATION OF THE USE OF SIMPLE CONCEPTS FOR PREDICTING THE SHAPE AND LOCATION OF DETACHED SHOCK WAVES

By Eugene S. Love

SUMMARY

A reexamination has been made of the use of simple concepts for predicting the shape and location of detached shock waves. The results show that simple concepts and modifications of existing methods can yield good predictions for many nose shapes and for a wide range of Mach numbers.

INTRODUCTION

In recent years interest has arisen in the problem of predicting the form and location of detached shock waves. This interest has been stimulated by the necessity for blunt noses and leading edges on configurations designed for hypersonic flight in order to cope with aerodynamic heating. The ability to predict the form and location of the detached shock is of primary importance in analyses of aerodynamic interference and aerodynamic heating. Knowledge of form and location also has a more elementary use in that it often influences the choice of maximum model size for a given wind tunnel. Numerous experimental and theoretical studies have been devoted to the determination of form and location as well as the important factors influencing form and location. (See refs. 1 to 36, for example.) Many of the studies have been centered upon particular important details of the problem and, therefore, have been logically restricted in scope, for example, studies restricted to hypersonic speeds or to regions in close proximity to the nose. Other studies have been more general in that they present methods for calculating detachment distance and shock shape without restrictions on speed or distance from the body. (See ref. 26, for example.) However, these methods usually involve laborious characteristic calculations or such lengthy iterative procedures that they have been evaluated only for one or two conditions, and, although the results obtained are good, less laborious methods are preferable if the results obtained by the simpler methods are satisfactory. A number of methods have, in the light of

subsequent experimental results, been shown to be inadequate (see the evaluations made in refs. 24 and 25, for example) or severely restricted in application (see ref. 18, for example).

With the aid of the theoretical and experimental information now available, a reexamination has been made of the more successful simple methods and concepts with a view toward (1) extending the range of applicability of existing methods through modification, (2) presenting simple methods for predicting shock shape and detachment distance, and (3) directing attention to areas where further study is needed. The results are presented in this paper. In the development of methods for prediction of shock shape and detachment distance, a primary objective has been to obtain results sufficiently accurate for most practical engineering applications. The methods presented are for air only (ratio of specific heats of 1.4) and are intended for use at supersonic and hypersonic speeds; the applicability of these methods at transonic speeds has not been examined to any extent.

SYMBOLS

b	distance between most forward point on shock and nose of body
C	constant defining detachment distance (see eq. (2))
C_c	value of C for convex face of complete hemisphere or two-dimensional semicircle symmetrically disposed with respect to free-stream direction
C_0	value of C for $\delta_0 = \delta_{det}$ (that is, $C_0 = 1$)
C_{90}	value of C for $\delta_0 = 90^\circ$ (flat face)
D	diameter of sphere or cylinder
d'	diameter or height in plane of point on body determined by angle for shock detachment
F	horizontal distance measured from center of spherical (or circular) nose or from face of flat nose to point on shock
M_∞	free-stream Mach number
q	slope defined by equation (3)

x	horizontal ordinate (free-stream direction)
x'	horizontal distance from most forward point on shock to plane containing d'
x_0	distance from most forward point of detached shock to intercept of its asymptote on X-axis (see fig. 9)
y	vertical ordinate (normal to free-stream direction)
$\beta = \sqrt{M_\infty^2 - 1}$	
γ	ratio of specific heats
δ_0	semiapex angle of cone (or wedge) or equivalent cone (or wedge)
δ_{det}	semiangle of cone (or wedge) for shock detachment
δ_s	flow deflection for sonic flow immediately behind shock
ϵ_s	local inclination of detached shock measured with respect to X-axis that gives sonic velocity behind shock
η	angle between normal to free-stream direction and control line (see fig. 9)
θ	angle between X-axis and line joining center of sphere (or cylinder) to corner of cut-off sphere (or cylinder)
μ_∞	free-stream Mach angle
ψ	term defined by equations (C7) and (C8)

DISCUSSION

Shock-detachment distance and its prediction will be considered prior to shock shape since the shape predictions hinge upon the detachment distance.

Shock-Detachment Distance

Review of general concepts.- It is instructive to review at the outset several well-known and fundamental features pertinent to shock detachment and detachment distance. To this end, consider the simple cone-cylinder (or wedge-slab) having a sharp shoulder at the juncture of the cone and cylinder and with a semiapex angle of δ_0 and an attached shock. As δ_0 is increased, the shock progresses continuously from a state of attachment to one of detachment in the manner described by Guderley (ref. 4) and by Busemann (ref. 5). As the value of δ_0 approaches that for detachment, a region of subsonic flow exists between the surface of the cone, the shock, and the sonic line the origin of which must of necessity be at the shoulder (refs. 4 and 5) which is the center of expansion to supersonic flow. Clearly, no part of the body downstream of the sharp shoulder affects the detachment process; and it becomes immediately apparent that the diameter at the shoulder d', and therefore the diameter at the sonic point of the body, is one of the fundamental parameters in determining detachment distance. For the cone-cylinder, the vertex of the detached shock for values of δ_0 barely larger than that producing detachment can be pushed no farther from the shoulder than the distance x' corresponding to the length of the cone that has a semiapex angle δ_{det}. Thus the maximum detachment distance (in the absence of viscous effects) is given by

$$\left(\frac{x'}{d'}\right)_{max} = 0.5 \cot \delta_{det} \qquad (1)$$

as has been previously inferred by Guderley (ref. 4) and others. Moeckel (ref. 9) refers to this expression as the geometric method for predicting detachment distance.

Inasmuch as equation (1) gives the maximum detachment distance, x'/d' must be expected to decrease as δ_0 varies from δ_{det} to larger values. From a physical viewpoint it may be reasoned that, as δ_0 increases beyond δ_{det}, the tip of the cone recedes toward the shoulder and loses contact with the shock; once contact is lost and as the cone tip recedes, the shape of the shock in the immediate vicinity of the nose adjusts itself to a shape of more uniform curvature in such a way that the peak in the detached shock that occurs when the cone tip is in close proximity to the detached shock (see shadowgraphs of ref. 27) is gradually eliminated and the front of the shock moves closer to the shoulder. The observations of Busemann (ref. 5) follow readily: there is no appreciable effect of nose shape upon detachment distance measured from the shoulder unless the nose tip is in close proximity to the detached shock;

and, except for the case of close proximity, the detachment distance and the shape of the detached shock between the sonic points on the shock are determined by the shoulder of the body. In order to locate the effective shoulders of bodies that have rounded noses, that is, bodies not having sharp shoulders of the type common to the cone-cylinder, Busemann proposes the use of the most upstream point on the body surface that is tangent to a line inclined at δ_{det} with respect to free-stream direction but also recognizes that, although this is the important point of the body, it is not in this case the location of the sonic point. This concept affords a simple means of correlating detachment distance for bodies of various shapes, and its general adequacy has been substantiated by experimental results (refs. 9 and 11, for example) for several different nose shapes and for Mach numbers up to about 3.

Compilation of and general correlation of data on detachment distance.- In the past few years, additional experimental information on detachment distance has been obtained and it is of interest to see whether these additional data may be correlated by the principle of Busemann. A compilation of experimental data according to this principle (that is, in terms of x'/d') is presented in figure 1. When these data were compiled, it was observed in several sources that some of the experimental data gave values of x'/d' that fell above the curve given by equation (1) (for example, some of the data of refs. 28 and 33). Since these points are believed to represent improbable values and were in a few instances recognized by the investigators as being associated with large experimental inaccuracies (ref. 33, for example), they have been omitted from figure 1. Where necessary, values of δ_{det} for converting the detachment distance to the form of x'/d' were obtained from reference 37.

The data of figure 1 show that the parameter x'/d' is a unifying one and is justified throughout the Mach number range of the experimental data shown. Similar conclusions of earlier studies in the supersonic speed range thus remain supported into the hypersonic speed range. Although the experimental data tend toward a single band of data for both the two-dimensional and axisymmetric compilations, there are differences at a given Mach number that can only be attributed to the effects of nose shape; examples of these effects and their prediction are shown subsequently. The continuity method of Moeckel (ref. 9) is seen to give a prediction that is in generally good agreement with the band of experimental data. The experimental data shown in figure 1 are for blunt nose shapes or for conditions where δ_0 is appreciably larger than δ_{det}. For spheres and for circular cylinders normal to the stream (two-dimensional), there is a geometric minimum x'/d' defined by the nose of the sphere and of the circular cylinder above which all experimental data must obviously lie. The curves defining these minimum values are

shown at the bottom of figure 1 in order to convey some idea of the proximity of the shock to the nose of these shapes.

Refinements for particular nose shapes.- On the basis of the available experimental data, certain refinements can be made that will enable a more accurate prediction to be made of detachment distance for certain nose shapes. A convenient basis for refinement is to modify the expression for the maximum nondimensional detachment distance as given by equation (1) to the following expression for the detachment distance under any condition:

$$\frac{x'}{d'} = 0.5C \cot \delta_{det} \tag{2}$$

In this expression the factor C is to be determined. The upper limit of C is obviously 1 (this limit will be designated C_0), and the lower limit will not be greatly removed from 1 in view of the secondary effects of nose shape and of the proximity to the curves for maximum detachment distance shown by the experimental data in figure 1.

Value of C for flat faces.- The value of C for flat faces will be designated as C_{90}. For axisymmetric bodies with flat faces, such as circular disks normal to the stream or the cone-cylinder with $\delta_0 = 90^\circ$, a value of $C_{90} = 0.70$ appears to give good agreement with experimental results over the Mach number range of the experimental data contained in figure 1. For infinite Mach number this simple conversion yields $x'/d' = 0.222$; this value compares favorably with a prediction of Serbin (ref. 16) for a circular disk normal to the stream and, when expressed in terms of the present parameters, yields 0.230 (shown to the far right in fig. 1). There is not as much experimental information on two-dimensional flat faces as for axisymmetric ones but, for the available two-dimensional data, a value of $C_{90} = 0.86$ appears to be satisfactory. (See fig. 1.) For an infinite Mach number this value yields $x'/d' = 0.421$ for a two-dimensional flat face.

Value of C for circular faces.- The value of C for the convex face the generatrix of which is the 180° (or greater) arc of a circle symmetrically disposed with respect to free-stream direction will be designated by C_c (the subscript c meaning complete to distinguish complete circular faces from modified circular faces to be considered subsequently). For complete circular faces, both axisymmetric and two dimensional, the value of C appears to vary significantly with Mach number. Figure 2 presents the variation of C_c with Mach number for the axisymmetric circular face (or sphere) and for the two-dimensional

circular face (or the circular cylinder normal to the stream). These curves were determined from the appropriate experimental data contained in figure 1. It will be noted that the curves have been extrapolated slightly beyond the range of the data contained in figure 1.

An interesting comparison can be made between the value of C_c for a sphere at hypersonic speeds as indicated by the curve of figure 2 and the values for detachment distance which Serbin (ref. 36) and Hayes (ref. 21) have calculated for a sphere for the case of M_∞ approaching ∞. The results of Serbin and Hayes may be expressed in terms of C_c. When this is done (and with $\gamma = 1.4$), Hayes' prediction yields $C_c = 0.825$ and Serbin's prediction gives $C_c = 0.850$; the latter value is in close agreement with the value $C_c = 0.857$ which the curve of figure 2 approaches at hypersonic speeds.

Variation for cone-cylinders and wedge-slabs.- For cone-cylinders having a semiapex angle δ_0 between δ_{det} and 90°, the refinement is not as readily obtained, but the recognition of certain features permits a prediction to be made of the effect of varying δ_0 between δ_{det} and 90°, and Johnston's experimental measurements of this effect (ref. 27) afford a ready means of checking a prediction. Consider first the variation of $\left(\frac{x'}{d'}\right)_{max}$ with δ_{det} as given by equation (1). If δ_{det} is replaced by δ_0 and $\frac{x'}{d'}$ is replaced by the cone length $\frac{x}{D}$, an expression for the variation in cone length with δ_0 is obtained. This variation is represented by the curve AA' in the following sketch:

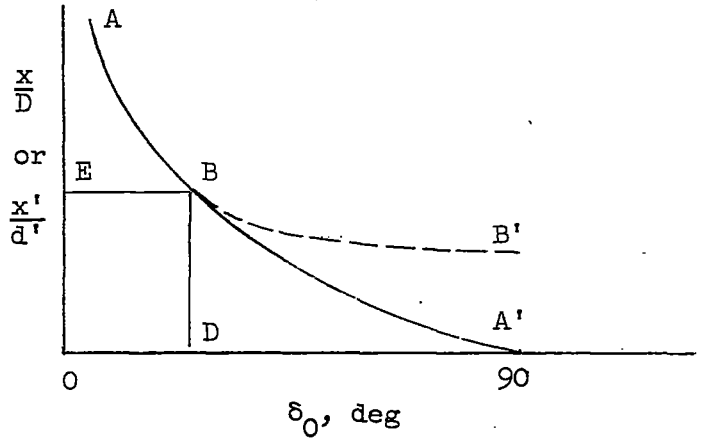

If the semiapex angle δ_0 of a cone-cylinder in a flow at constant supersonic Mach number is allowed to increase continuously from some

very small value to 90°, the following conditions occur. At first the shock is attached and the distance $\frac{x}{D}$ between the shoulders of the cone-cylinder and the vertex of the attached shock varies according to the curve AA'. However, when δ_0 reaches δ_{det} (point D) corresponding to the given Mach number, the distance between the vertex of the shock and the shoulder ceases to vary according to the curve AA'. The value of $\left(\frac{x'}{d'}\right)_{max}$ for a detached shock (point E) has been reached and, with a further increase in δ_0, $\frac{x'}{d'}$ must decrease according to some curve, say BB', which defines the variation in detachment distance. It is apparent that an infinite number of curves of the type BB' may branch off from the curve AA', since for every value of M_∞ there is a corresponding curve BB'. Point B will never reach A' since for $M_\infty = \infty$ the value of δ_{det} is 57.6° for cones (after Maccoll, ref. 35) and about 45.6° for wedges. The problem is thus one of determining the general form of the curve BB'.

Guderley (ref. 4) has shown that the transition from attached shock to detached shock is one of continuous change. Therefore, it is reasonable to assume that at point B the slope of the curve BB' will be equal to the slope of the curve AA'. This slope will be designated by q and, from equation (1), it has the value

$$q = -0.5 \csc^2\delta_{det} \tag{3}$$

Thus the ordinates and slope of the curve BB' at point B can be calculated. When $\delta_0 = 90°$ (point B'), the detachment distance x'/d' corresponds to the flat-face condition for which empirical values of C in equation (2) have already been proposed. The slope of the curve BB' at B' must be essentially zero, if not exactly so. Thus the ordinates and slope at both ends of the curve BB' are obtainable. From the works of Guderley and Busemann, the form of the curve BB' must be such that x'/d' is always decreasing and the rate of decrease in x'/d' with δ_0 is greatest at δ_{det}. Consequently, from the knowledge of the end-point conditions and the restrictions on the form of the curve, one is led to suggest that the curve BB' is close to being elliptic in form. The development of the general elliptic equation giving the variation in x'/d' between $\delta_0 = \delta_{det}$ and $\delta_0 = 90°$ is given in appendix A.

Predictions of the variation in detachment distance for cone-cylinders and wedge-slabs (two-dimensional) according to appendix A

are given in figure 3 for several Mach numbers, and comparisons are made between Johnston's experimental results (ref. 27) at $M_\infty = 2.45$ and the predicted variations for this Mach number. The predicted variations agree closely with the experimental results. The two-dimensional wedge data fall slightly above the predicted curve; however, one suspects that this difference may be attributed to the difficulty in obtaining two-dimensionality in experimental investigations of this type (see refs. 11, 24, 25, and 26, for example) since the experimental data for the wedge do not show the correct values of $\left(\frac{x'}{d'}\right)_{max}$ for δ_{det} at $M_\infty = 2.45$. Further, the experimental data for the wedge are, in general, uniformly higher than the predicted curve by the amount of the experimental error at δ_{det}.

The same procedure as employed for the prediction of figure 3 may be used to calculate the variation in x'/d' with M_∞ for constant δ_0. Examples of this prediction are given in figure 4 for a cone-cylinder at several values of δ_0. No suitable experimental data for cone-cylinders were found for comparison; however, the results of figure 3 lend validity to the predictions of figure 4, and the experimental results of Griffith (ref. 28) for wedges tend to substantiate the type of variation shown here when M_∞ is decreased below that for detachment.

Variation for cut spheres and cylinders.- One interesting model that has been used in the study of detachment distance is the so-called cut sphere (axisymmetric case) or cut cylinder (two-dimensional case). The cut sphere or cylinder is so termed because the shape of the sphere or cylinder is altered by actually cutting segments from the sphere or cylinder or the models are so constructed that they simulate the effect of this cutting. For example, the diameter of a hemisphere-cylinder may be reduced by concentric machining such that the nose shape varies systematically from a hemisphere to a flat face (of zero diameter in this limit, however). The nondimensional results thus obtained (with the exclusion of the zero-diameter limit) can be considered to be the same as those that would be obtained, for example, with a number of models of constant diameter and with varying radius of the nose. A similar procedure is applicable to the circular cylinder normal to the stream (two-dimensional) which in the case of actual cutting amounts to removing symmetrically disposed segments along parallel planes that are also parallel to the plane of symmetry and to the free-stream direction.

The cut sphere or cylinder is thus seen to afford a convenient means for examining the effect upon detachment distance of systematically varying the radius of the nose while diameter or height is held constant,

and thus a range of interesting nose shapes is covered. Further, one is able to determine the radial point on a sphere or cylinder that is most important in fixing detachment distance.

In reference 24, Kim reports the results of two-dimensional tests of a cut cylinder at $M_\infty = 4$. However, in reference 24 there are some discrepancies in the figures and in the values tabulated and those indicated in the figures of that reference. In order to justify the corrections that are made herein to account for the discrepancies appearing in reference 24, the shock shapes as reported by Kim are reproduced herein in figure 5. In order to agree with Kim's tabulated values, the abscissa scale would need to be condensed as shown. With this modification a check is obtained of Kim's quoted values except for $\theta = 30^\circ$, for which a value of 0.20 is indicated. (See tabulation at top of figure 5.) Kim's results are expressed in the ratio of the distance between the shock and the nose to the diameter of the complete or uncut cylinder ($\theta = 90^\circ$). Although this ratio is an irrelevant one from an analytic viewpoint, its use is more appropriate here than the use of the correlating form x'/d', since the object is to determine the critical value of θ which in essence is determining d'. (The critical value of θ defines the point on the nose that separates the portion of the nose that affects detachment distance from the portion that does not.) Further, by use of Busemann's concept of d' and a few simple assumptions, it is possible to calculate the variation of b/D with θ. In order to calculate this variation within the framework of the previous methods employed herein, one recognizes at the outset that the value of C for the uncut cylinder (or sphere) ($\theta = 90^\circ$) is different from the value of C for the flat face ($\theta = 0^\circ$). The variation in C between these two limits is thus needed. As a first approximation it may be assumed that this variation is linear; from this assumption it follows that

$$C_c = C_{90} + \theta \frac{dC}{d\theta} \tag{4}$$

where C_c is the value of C for the complete cylinder (or sphere), $dC = C_c - C_{90}$, C_{90} is the value of C for the flat face, and $d\theta = 90^\circ - \delta_{det}$. From the previously presented values of C_c and C_{90}, the linear variation of C with θ is easily obtained. With the aid of equation (2), the variation of x'/d' with θ may be calculated and converted to terms of b/D by the following equation:

$$\frac{b}{D} = \frac{x'}{d'} \sin\theta + \frac{\cos\theta}{2} - \frac{1}{2} \tag{5}$$

where $0^\circ \leq \theta \leq 90^\circ - \delta_{det}$. For values of θ between 90° and $90^\circ - \delta_{det}$, the present analysis gives constant values of b/D at the value calculated for $\theta = 90^\circ - \delta_{det}$. (Note that, for this statement and for equation (5), D is the diameter of the uncut model.)

From the results of figure 3, an elliptic variation of C would appear to be a more justifiable and accurate representation than the linear one. The method for computing the elliptic variation is covered in appendix B.

Figure 6 presents the calculated linear and elliptic variations of C for the two-dimensional cylinder of Kim's experiments at $M_\infty = 4$. Also shown for comparison is the variation in C for wedge-slabs between $\delta_0 = \delta_{det}$ and $\delta_0 = 90^\circ$ as considered previously. For convenience, both θ and δ_0 are shown as the abscissa, θ being merely $90^\circ - \delta_0$.

Figure 7 presents Kim's experimental measurements and compares them with the present predictions. The correction to the experimental point at $\theta = 30^\circ$ as shown by figure 5 is included in figure 7, as is a correction to the point at $\theta = 42^\circ$ which is apparently misplotted in a similar figure in reference 24 since it does not agree with the quoted value in reference 24 or the value obtained from the shock locations (reproduced in fig. 5 herein). Of the present predictions the linear variation of C gives the better agreement with Kim's data fairing but this seems to be meaningless for the reasons just stated. When the data are plotted according to what are believed to be the correct values, the elliptic prediction is to be preferred and probably lies within the accuracy of the experimental data. Kim justifies the critical value of $\theta = 48^\circ$, obtained by extrapolation, on the grounds that the critical value of θ must coincide with "the foot of the last Mach line" or sonic line, and in support of this statement quotes a calculated critical value of θ of 44°. However, in view of the fact that the value of $\theta = 48^\circ$ was obtained by extrapolation of a faired curve through apparently erroneous points, as shown in figure 7 herein, this argument is weakened. The present predictions place the critical value of θ at 51.2° (which is $90^\circ - \delta_{det}$ as dictated by Busemann's concept). It is not only possible but highly probable that the foot of the sonic line occurs at $\theta < 51.2^\circ$ for, as Busemann has pointed out in reference 5, a peculiarity of the detachment phenomena is that the critical point which plays the primary role in fixing detachment distance for arbitrarily rounded nose shapes turns out to be situated where the flow is purely supersonic. Both the foot of the sonic line and the foot of the last characteristic which intersects the sonic line are ahead of this

critical point. However, as also pointed out in reference 5, the body slope must decrease to smaller angles than δ_{det} if the sonic line is to complete its enclosure of the subsonic region behind the shock. Thus what at first glance appears to be a peculiarity actually is a fulfillment of a necessary condition.

One may reasonably inquire as to the difference that there would have been in the predictions of b/D in figure 7 if no account had been made for the change in C from C_{90} to C_c. A brief examination shows that the predictions would suffer considerably. For example, if C had been held constant at C_{90}, b/D would have been 0.23 at $\theta = 51.2^\circ$ instead of 0.269.

Recently, Mr. Robert W. Rainey of the Langley Laboratory has obtained results (unpublished) for a series of axisymmetric shapes at $M_\infty = 3.55$ in which the diameter was held constant and the radius of the nose was varied in such a way that the nose shapes varied from a hemisphere to a flat face. These results are particularly interesting since they include data for a value of θ very close to the critical value predicted by the Busemann concept $(90^\circ - \delta_{det})$. The data are again presented in terms of b/D rather than x'/d' in order to bring out an important feature of this type of presentation. These results are shown in figure 8 and are compared with the predicted curve employing an elliptic variation of C determined according to appendix B. Values of x'/d' thus obtained may be converted to b/D values by the relation

$$\frac{b}{D} = \frac{x'}{d'} + \frac{1}{2 \tan \theta} - \frac{1}{2 \sin \theta} \tag{6}$$

for $0^\circ \leqq \theta \leqq 90^\circ - \delta_{det}$ and by the relation

$$\frac{b}{D} = \frac{\sin (90^\circ - \delta_{det})}{\sin \theta} \left[\frac{x'}{d'} + \frac{1}{2 \tan (90^\circ - \delta_{det})} \right] - \frac{1}{2 \sin \theta} \tag{7}$$

for $90^\circ - \delta_{det} \leqq \theta \leqq 90^\circ$. (Note that, for these equations and for the experimental models of fig. 8, D is effectively the diameter of cut models as contrasted to the results of fig. 7; thus, b/D is not constant for values of θ between 90° and $90^\circ - \delta_{det}$ as in fig. 7.)

The prediction shows excellent agreement with the experimental results, and the experimental results confirm the existence of a predicted knee at $\theta = 90^\circ - \delta_{det}$, in this case at 38.5°. The Busemann concept of the most important point of an arbitrary blunt profile being determined by δ_{det} is once again clearly substantiated. The results of figure 8 should serve to correct the impression left by less complete experiments that the variation of b/D with θ between 0° and 90° occurs smoothly and without a knee near $\theta = 90^\circ - \delta_{det}$.

Shape of Detached Shocks

Initial considerations.- When the methods that have been proposed for predicting shock shape which do not involve laborious procedures were examined, the method of Moeckel (ref. 9) appeared to offer the best possibility, when modified, for giving satisfactory predictions at both supersonic and hypersonic speeds for nose shapes that do not approach too closely the condition of attached shock. This method has been shown to give generally satisfactory results at supersonic speeds (see refs. 9 and 11, for example) but is known to be inadequate in its present form at hypersonic speeds. The method is proposed only for that region of the shock between the sonic points; however, Moeckel's experimental results show that the method may for many nose shapes be satisfactory as an approximation of the shock shape at distances considerably beyond the sonic points on the shock.

Before modifications are discussed, it would perhaps be worthwhile to review briefly Moeckel's method. (See ref. 9.) In this method it is assumed that the shock shape is hyperbolic in form and that its location and scale in relation to the body are determined from continuity considerations involving certain assumptions. These assumptions include the location of the sonic point on the body by the use of δ_{det}, the use of a straight sonic line, and the determination of the sonic point on the shock by assuming the straight sonic line to be inclined at an angle η with respect to the vertical where η is equal to $\frac{1}{2}(\delta_{det} + \delta_s)$ and δ_s is the deflection of the flow at the sonic point on the shock. As has been recognized by Moeckel, two severe assumptions of his method are the use of a straight sonic line and the sonic line being inclined at $1/2(\delta_{det} + \delta_s)$.

Development of present method.- In the present development, major modifications are made to Moeckel's method. The continuity relation is not used, and only the trigonometric derivations are retained. The present method employs the results of the first part of this paper to calculate detachment distance instead of the continuity relation of

reference 9. Secondly, the straight line arising from the point on the body determined by δ_{det} (see fig. 9) and determining the point on the shock where the shock inclination ϵ_s is equal to that for sonic velocity behind the shock is not restricted in inclination to a value of $\eta = 1/2(\delta_{det} + \delta_s)$. Further, this straight line is not regarded as being a sonic line but as a control line that reproduces the effects of the true sonic line. There are several reasons for this assumption. The sonic point on the body lies ahead of that given by δ_{det} (except for the case of the sharp shoulder), and the exact sonic line is curved and according to reference 26 is, as a general rule, not normal to the stream lines at the sonic points on the body and at the shock; neither is it necessarily normal to the streamlines between these points. It is clear then that a straight control line which reproduces the effects of the true sonic line will not satisfy the inclination of the true sonic line at both of its extremities nor, as a general rule, is the control line likely to be inclined at the mean of the inclinations at the two extremities of the true sonic line. Further, the inclination η of the control line that most effectively reproduces the influence of the true sonic line will not necessarily be that which gives a line that appears to represent best the actual location or average inclination of the true sonic line. It follows that the determination of the value of η for the control line by analytic methods would be difficult. However, since the publication of Moeckel's work (ref. 9), a large number of experimental shock shapes have been obtained over a wide range of Mach number. With these experimental results and the advantage of hindsight, together with an expression for η derived from Moeckel's trigonometric relations, one is able to determine values of η from known shock shapes. This expression for η is given in appendix C, as are simple relations for converting shock ordinates for circular and flat noses. Several calculations of η quickly revealed that the hyperbolic form of shock shape is best adapted to the spherical or circular nose (rather than the flat) when it is desired to obtain a value of η that is suitable for shock shape both near to and far from the nose. Consequently, attention was centered upon obtaining the variation in η for spherical and circular (two-dimensional) noses. In order to determine a value of η for a given Mach number, calculations were made for several points along the shock and the average was taken of the resulting values of η. In general, the calculated values of η ranged approximately $\pm 6^\circ$ about the average value at the higher Mach numbers with less scatter at the lower Mach numbers. It is important to note that, whereas the value of η is obtained by means of the tangent function (see eq. (C3) of appendix C), and therefore varies within the limits of the principal values of the tangent ($\pm 90^\circ$), the actual movement of the control line (fig. 9) is such that η rotates continuously counterclockwise with increasing M_∞. Thus negative angles (calculated from eq. (C3)) have

been converted to their positive complements ($>90^\circ$ but $<180^\circ$) to achieve compatibility with the rotation of the control line.

Variation of η with M_∞.- The variation of η obtained by the above procedure is shown in figure 10 for the sphere and the circular cylinder (two-dimensional) together with the values of δ_{det}, δ_s, and Moeckel's value of $1/2(\delta_{det} + \delta_s)$. The adequacy of the values of η obtained in the present analysis will be shown subsequently by using these values in the calculations of shock shapes and comparing these calculated shapes with a number of the experimental shapes. The experimental shapes will include some of those from which points were taken to calculate the average η-values. The striking feature of figure 10 is the increasingly large difference between Moeckel's values (given by $\eta = 1/2(\delta_{det} + \delta_s)$) and those of the present analysis. For spheres, the present analysis gives values of η that are always greater than $1/2(\delta_{det} + \delta_s)$; near $M_\infty = 8$ the present values are about $2\frac{1}{2}$ times greater. For two-dimensional circular cylinders, the present values fall below $1/2(\delta_{det} + \delta_s)$ at the lower Mach numbers and above, at the higher Mach numbers. With regard to these comparisons with Moeckel's results, it should be recalled that his method is proposed only for the region between the sonic points of the shock, whereas the present analysis attempts to include the shock beyond the sonic points as well. There was some indication that the values of η determined in the present analysis would be smaller than those shown if the analysis had been confined to the portion between the sonic points; however, these smaller values would still be much larger than $1/2(\delta_{det} + \delta_s)$ at the higher Mach numbers.

Shown in the upper right-hand part of figures 10(a) and 10(b) are three values of η that may be indicative of the magnitude to be expected at infinite Mach number. The value designated tangential η corresponds to the condition for which the control line becomes parallel to the nose surface at its point of origin on the surface (that is, $90^\circ + \delta_{det}$). The value designated as being determined from C_c corresponds to the condition for which the control line intersects the axis of symmetry at the vertex of the shock whose detachment distance is determined from the value that C_c tends to obtain at hypersonic speeds in figure 2 ($C_c = 0.857$ for spheres and 0.952 for cylinders); this condition implies that the sonic point on the shock is at the vertex of the shock. The value designated maximum η corresponds to the condition of the control line passing through the tip of the nose on the axis of symmetry; this condition implies that the shock touches the nose, that the sonic point on the shock is at the vertex of the shock, and therefore

that the sonic points on the shock and on the nose coincide. The conditions associated with maximum η and η determined from C_c require the control line to pass through the body; this passage through the body is not a point for concern since the control line was proposed as reproducing the effect of the sonic line and not as simulating its location or its termini.

Some interesting similarities exist between the variation in η, or more properly, the control-line termini obtained in the present analysis and the termini of the sonic line obtained by Serbin (ref. 36), Chester (ref. 31), and apparently by Freeman (ref. 32). Chester's analysis shows explicitly that for all values of γ the position of the sonic point on the body does not experience large changes as M_∞ increases from moderate supersonic speeds to speeds approaching infinity, whereas for all values of γ except unity the sonic point on the shock experiences significant changes and moves toward the vertex of the shock. (For $\gamma = 1$, the sonic point on the shock is indicated to be at the vertex of the shock.) Thus, for γ other than unity, these variations of the sonic points are of the same type as the variations exhibited by the termini of the control line in the present analysis. Both Serbin's and Chester's analyses indicate that, when $M_\infty = \infty$ and $\gamma = 1$, the sonic point on the shock is at the vertex of the shock, the detachment distance is zero, and the sonic points on the shock and on the body coincide (same sonic point conditions as discussed in the preceding paragraph for maximum η). For $M_\infty = \infty$ and $\gamma = 1.4$, the same analyses indicate a finite detachment distance and the sonic point on the shock and on the body to be removed from the axis of symmetry. For comparison with the control line inclination of the present analysis, a straight line connecting the sonic points of Chester's analysis would be inclined at 90° with respect to the vertical. Thus, although some interesting similarities are observed between the locations and movements of the sonic points of these analyses and the behavior of the control-line inclination and termini of the present analysis, there are also differences that remind one not to lose sight of the major differences between the true sonic line and the control line, as pointed out previously.

Effect of C and η upon shock shape.- The procedure for calculating the shock shape is outlined in appendix D. It is of interest to examine at the outset the effects of changes in C and η upon shock shape. This is done in figures 11 and 12 by comparing the various predictions with experimental results at $M_\infty = 1.94$ for a hemisphere-cylinder. Figure 11 presents the shock shape in terms of d' and with horizontal distance referenced to the vertex of the shock in the form $\frac{x}{d'} - \frac{x_0}{d'}$. (See fig. 9.) This is the same form employed by Moeckel

in his evaluation of his predictions in references 9 and 11. Figure 12 presents the shock shape in terms of the maximum diameter D and with the horizontal distance referenced to the center of the sphere F/D.

The results of figure 11 show readily (as do the results of fig. 12 by closer examination) that, although C was developed as a means for obtaining detachment distance, it also has a significant influence on shock shape. Figure 11 also shows that, when this form of presentation is used, one may obtain an almost identical prediction with different combinations of η and C and that these combinations would give an excellent prediction of the experimental shock shape (not to be confused with shock location). One may immediately conclude that, although this form of presentation is convenient for isolating the effects of C, it could lead to ambiguities and thus is not in itself always adequate in the present analysis to evaluate the predictions of shock shape. Accordingly, the form of presentation shown in figure 12 has been used. In this figure are shown the effects of C upon shock shape and location for $\eta = 1/2(\delta_{det} + \delta_s)$ within the C-limits established herein (1.0 and 0.7) for axisymmetric noses and the effects of η upon the shock shape for the value of $C_c = 0.804$ determined herein for spheres at $M_\infty = 1.94$. (See fig. 2.) With $C_c = 0.804$, the position of the shock at the nose is, as is to be expected, accurately given. With increasing η (from δ_s, to Moeckel's value, to δ_{det}, and finally to the value given by fig. 10), the shock curves downstream more rapidly and the prediction given by the present analysis ($\eta = 44^\circ$ from fig. 10) is in excellent agreement with the experimental results. The prediction given by $\eta = \delta_{det}$ is also good at this Mach number and the prediction given by $\eta = 1/2(\delta_{det} + \delta_s)$ is fair. From these results and from figure 10, one sees some basis in the past practice of replacing $1/2(\delta_{det} + \delta_s)$ by δ_{det} when Moeckel's method is used; figure 10 shows that δ_{det} and the curve of the present analysis are in close agreement below about $M_\infty = 2$, and above this Mach number the curve for δ_{det} is always nearer the curve of the present analysis. However, at high Mach numbers this is indeed a trivial point. One also sees why the use of Moeckel's value gives reasonable predictions at low Mach numbers, particularly over that portion of the shock near the nose for which it was intended.

Examples of shock prediction by present method.- Numerous calculations have been made by the present method of the location and shape of detached shocks. These calculations have been compared with experimental results, and some additional random evaluations of changing η have been made. Some examples of these comparisons and evaluations are shown in figures 13 to 17.

Figure 13 reproduces the shocks obtained by Kim (ref. 24) on a two-dimensional circular cylinder at Mach numbers from 1.35 to 6. Shown for comparison are the predicted shocks with $\eta = \delta_{det}$, which in essence equals Moeckel's value of $1/2(\delta_{det} + \delta_s)$ for two-dimensional flow, and with η given by figure 10(b). With $\eta = \delta_{det}$ or $1/2(\delta_{det} + \delta_s)$, the predicted shocks curve rearward too rapidly at low M_∞ and too slowly at high M_∞. For example, examine shock shapes at $M_\infty = 1.8$ and $M_\infty = 6$. With η varying according to figure 10(b), the predicted shocks are in much closer agreement with the experimental shocks at all Mach numbers. Figure 15(a) also contains two-dimensional results and shows excellent agreement between prediction and experiment.

Figures 14(b), 15(b), 16(a), and 17 compare the predicted shocks with the experimental shocks for hemisphere cylinders for Mach numbers of 3.55, 5.8, 6.8, and 7.7, respectively. In all instances the present prediction agrees well with experiment. Figure 16(a) also includes the prediction with $\eta = \delta_{det}$ to demonstrate the increasingly large disagreement with experiment that accompanies the use of this value of η with increasing M_∞; a prediction with $\eta = 1/2(\delta_{det} + \delta_s)$ would show larger disagreement with experiment.

Figures 14(a) and 16(b) show what may be expected in the way of predicting the shock for flat-face cylinders alined with the flow at $M_\infty = 3.55$ and 6.8, respectively, by converting the corresponding predicted shocks for a hemispherical nose (figs. 14(b) and 16(a)) by use of the Busemann concept. For the flat-face condition d' becomes D and coincides with the location of the flat face. Thus, the necessary conditions for conversion are simply

$$\left(\frac{y}{D}\right)_{flat} = \left(\frac{y}{d'}\right)_{spherical\ or\ circular} \tag{8a}$$

and

$$\left(\frac{F}{D}\right)_{flat} = \left(\frac{x}{d'} - \frac{x_0}{d'} - \frac{x'}{d'}\right)_{spherical\ or\ circular} \tag{8b}$$

The resulting shock shapes for the flat face obtained by this conversion are not in good agreement with the experimental shocks, particularly at large distances from the nose. However, some disagreement is to be expected. The values of η for a flat face would probably be less than those for a round nose in view of the influence of the sharp shoulder of the flat face in defining the area between the

shock and the nose where the flow is choked. Further, the disagreement at large distances from the nose is in the direction to be expected since the sharp shoulder of the flat face is the source of a centered expansion which interacts with the shock in a manner that reduces its inclination more rapidly than would the gradual expansion from the spherical (or circular) nose. There is also the possibility that the sharp shoulder produces a separation bubble and an associated overexpansion, but experimental evidence on this point is at present not sufficient to indicate its significance at moderate or high Mach numbers. In spite of these shortcomings, it would appear reasonable to regard this prediction as a suitable first-order prediction for flat faces. The important point to be gathered from these flat-face predictions is that they indicate the maximum discrepancy that may be expected in predicting shock shape by means of the spherical (or circular) calculation for noses that vary all the way from hemispherical to flat shapes (in the manner of the nose shapes of fig. 8). As the nose shape departs from the flat and moves toward the hemispherical, the agreement between prediction and experiment becomes increasingly good.

Figure 17 compares the present prediction with the experimental results at $M_\infty = 7.7$ presented by Lees and Kubota in reference 22 for a hemisphere-cylinder. Also shown are the predictions made in reference 22 by means of blast-wave theory. The present prediction is in excellent agreement with the experimental shock.

Shock shapes for blunted cones.- The blunted cone with flat or rounded tip has become increasingly common in hypersonic vehicles. Attempts were made to adapt the present method of prediction to the general case of truncated cones but with little success. Characteristic reflection methods similar to those mentioned by Giese and Bergdolt (ref. 29) proved to be inadequate primarily because methods that were suitable for estimating the overexpansion and subsequent convergence toward conical flow at low Mach numbers were completely inadequate at high Mach numbers (and vice versa). Nevertheless one point of possible convenience was exposed. So long as the semicone angle of the blunted cone does not exceed about 15° for Mach numbers in the neighborhood of 3 and below, decreasing to about 8° at Mach numbers near 8, the effect of overexpansion in producing a reflex in the shock shape is negligible for all practical purposes, and the shock may be calculated by the usual procedure with the additional condition that, when its slope deteriorates to that which would be produced by the cone in the absence of tip bluntness, the slope is maintained constant at this value.

CONCLUDING REMARKS

A reexamination has been made of the use of simple concepts for predicting the shape and location of detached shock waves. The results show that simple concepts and modifications of existing methods can yield good predictions for many nose shapes and for a wide range of Mach numbers.

Langley Aeronautical Laboratory,
National Advisory Committee for Aeronautics,
Langley Field, Va., August 28, 1957.

APPENDIX A

DEVELOPMENT OF GENERAL ELLIPTIC EQUATION GIVING THE VARIATION IN DETACHMENT DISTANCE BETWEEN $\delta_0 = \delta_{det}$ AND $\delta_0 = 90^\circ$ FOR CONE-CYLINDERS AND WEDGE-SLABS

Consider the general elliptic equation

$$\frac{1}{a^2}(x - l)^2 + \frac{1}{b^2}(y - k)^2 = 1 \tag{A1}$$

with center at l,k and semiaxes a and b.

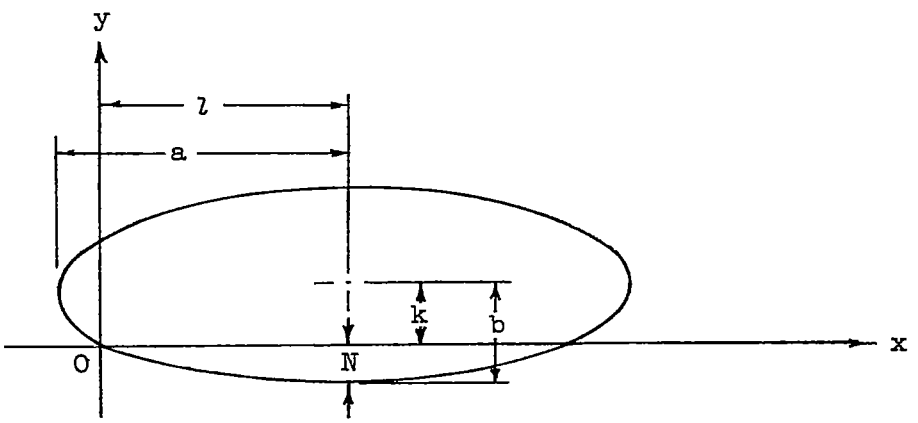

From the sketch

$$k = b + N \tag{A2}$$

Differentiating equation (A1) with respect to x and substituting equation (A2) into it yields

$$\frac{dy}{dx} = -\frac{b^2}{a^2}\frac{x - l}{y - (b + N)} \tag{A3}$$

If the slope at $x = 0$, $y = 0$ is denoted by q, then from equation (A3) it follows that

$$a^2 = -\frac{b^2 l}{q(b + N)} \tag{A4}$$

Also at $x = 0$, $y = 0$, substituting equation (A2) into equation (A1) yields

$$a^2 = \frac{l^2 b^2}{b^2 - (b + N)^2} \tag{A5}$$

Equating (A4) and (A5) gives

$$b = \frac{lqN - N^2}{2N - lq} \tag{A6}$$

Equation (A1) may be expressed as

$$\left(\frac{1}{b^2}\right)y^2 - \left[\frac{2(b + N)}{b^2}\right]y + \left[\frac{(b + N)^2}{b^2} + \frac{1}{a^2}(x - l)^2 - 1\right] = 0 \tag{A7}$$

which is readily recognized as a quadratic, the solution for which is easily obtained. In terms of the shock-detachment parameters, the constants and variables involved in the solution of equation (A7) are

$$\left.\begin{aligned} x &= \frac{\delta_0 - \delta_{det}}{57.3} \\ l &= \frac{90 - \delta_{det}}{57.3} \\ q &= -0.5 \csc^2\delta_{det} \\ N &= p\left(C_{90} - 1\right) \end{aligned}\right\} \tag{A8}$$

where $p = 0.5 \cot \delta_{det}$ and C_{90} is the value of C for $\delta_0 = 90^\circ$ or the flat-face condition; that is, $C_{90} = 0.70$ for cone-cylinders and $C_{90} = 0.86$ for wedge-slabs (two-dimensional).

Values of x are determined by allowing δ_0 to vary between δ_{det} and 90°. The corresponding values of y calculated from equation (A7) are converted to the detachment distance parameter x'/d' by

$$\frac{x'}{d'} = p + y \tag{A9}$$

APPENDIX B

METHOD FOR CALCULATING ELLIPTIC VARIATION OF C FOR CUT CYLINDERS AND SPHERES

Consider first a typical variation of x'/d' for a cone-cylinder (or wedge-slab) as δ_0 varies between δ_{det} and 90°, that is, the curve BB' in the following sketch:

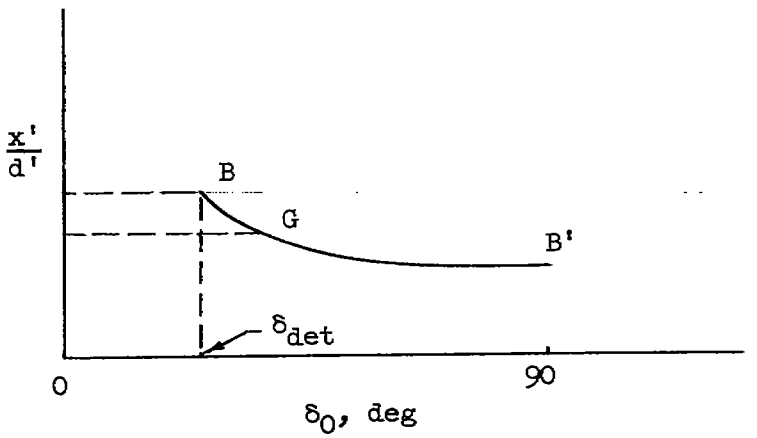

As shown previously, the maximum value of x'/d' occurs at point B and at this point $C = 1$. The minimum value of x'/d' occurs at point B' and at this point C is equal to that for a flat face or C_{90}. It is readily recognized that C_{90} and point B' also apply to the case of the cut sphere (or cylinder) for $\theta = 0°$, where $\theta = 90° - \delta_0$, since as θ approaches 0° the cut sphere approaches a flat face (limit of $\theta = 0°$ excluded); or alternatively, for the case of constant maximum diameter D and varying nose radius R, $R/D = \infty$ when $\theta = 0°$ and the face is flat.

The value of C for the complete sphere (that is, C_c) is always less than 1, and the corresponding value of x'/d' may be denoted on the curve BB', for example, at point G. The value of δ_0 corresponding to point G is incidental to the development herein, since it merely defines the cone-cylinder giving the same detachment distance as the complete sphere. The importance of point G lies in the slope at this point. For the cut sphere the slope $dC/d\delta_0$ and the value of C at $\delta_0 = 90°$

are known as is the value of C at $\delta_0 \leqq \delta_{det}$; in line with the Busemann concept C is assumed to be equal to C_c for $\delta_0 \leqq \delta_{det}$. Thus the only quantity needed to determine the elliptic variation (assumed) in C for the cut sphere is the slope $dC/d\delta_0$ at δ_{det}. No ready solution was found for this slope (as contrasted to that for cone-cylinders), but it is likely close to that which may be determined from the curve BB' at point G. The assumption is therefore made herein that the slope $dC/d\delta_0$ for the cut sphere at δ_{det} is equal to that which may be determined from this point. The variation of C for the cut sphere in comparison with that for the cone-cylinder may thus be sketched:

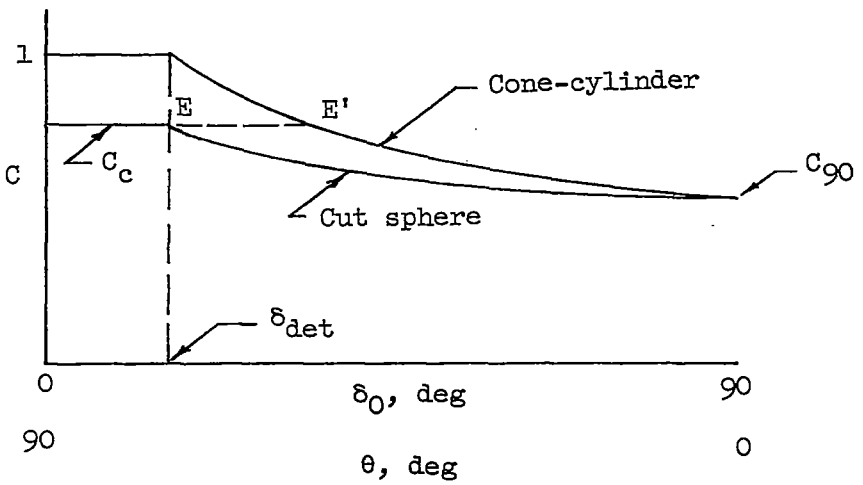

and the slope at E is equal to the slope at E'.

The procedure for calculating the elliptic variation is as follows: Determine the value of C_c at the particular value of M_∞ from figure 2. Substitute this value of C_c into the following expression and obtain y:

$$y = p(C_c - 1) \tag{B1}$$

where $p = 0.5 \cot \delta_{det}$. Substitute y into the elliptic equation (derived in appendix A) and solve for x:

$$\left(\frac{1}{b^2}\right)y^2 - \left[\frac{2(b + N)}{b^2}\right]y + \left[\frac{(b + N)^2}{b^2} + \frac{1}{a^2}(x - l)^2 - 1\right] = 0 \tag{B2}$$

where, as in appendix A,

$$\left.\begin{aligned} a^2 &= -\frac{b^2 l}{q(b+N)} \\ b &= \frac{lqN - N^2}{2N - lq} \\ q &= -0.5 \csc^2 \delta_{det} \\ l &= \frac{90 - \delta_{det}}{57.3} \\ N &= p\left(C_{90} - 1\right) \end{aligned}\right\} \tag{B3}$$

and $C_{90} = 0.86$ for the two-dimensional case and $C_{90} = 0.70$ for the axisymmetric case.

Although it is not required in this procedure, if one desires the value of δ_0 corresponding to the complete sphere (or cylinder), it may be obtained by substituting this calculated value of x into the general relation

$$x = \frac{\delta_0 - \delta_{det}}{57.3} \tag{B4}$$

Next, with the value of y from equation (B1) and the value of x from equation (B2), calculate dy/dx from

$$\frac{dy}{dx} = -\frac{b^2}{a^2}\left[\frac{x - l}{y - (b + N)}\right] \tag{B5}$$

This value of dy/dx equals $\dfrac{d\left(\frac{x'}{d'} - p\right)}{d\left(\frac{\delta_0 - \delta_{det}}{57.3}\right)}$ which in turn equals

$\frac{d\left(\frac{x'}{d'}\right)}{d\delta_0}$. And since

$$\frac{dC}{d\delta_0} = \frac{1}{p} \frac{d\left(\frac{x'}{d'}\right)}{d\delta_0} \tag{B6}$$

the value of dy/dx from equation (B5) may be substituted into the following equation:

$$\frac{dC}{d\delta_0} = \frac{1}{p} \frac{dy}{dx} \tag{B7}$$

to obtain $dC/d\delta_0$ which is the desired slope at E and E'. (See sketch.)

It now remains to determine the variation of C with δ_0 (or θ). In order to do this, the elliptic equation (B2) is used, but note that the constants q and N are now

$$\left.\begin{aligned} q &= \frac{dC}{d\delta_0} \\ N &= C_{90} - C_c \end{aligned}\right\} \tag{B8}$$

and therefore a^2 and b are also different. From equation (B4) and the relation $\delta = 90^\circ - \theta$,

$$x = \frac{(90^\circ - \theta) - \delta_{det}}{57.3} \tag{B9}$$

Let θ vary from 0° to $90^\circ - \delta_{det}$, substitute the corresponding values of x into the elliptic equation with the indicated change in constants, and solve for y.

Obtain values of C from

$$C = C_c + y \tag{B10}$$

Substituting these values of C into

$$\frac{x'}{d'} = Cp \tag{B11}$$

gives the variation of x'/d' with θ $\left(\text{or } \delta_0\right)$.

APPENDIX C

DERIVATION OF METHOD FOR CALCULATING η FOR KNOWN SHOCK SHAPES

The following quantities are known or can be determined according to the methods suggested in the text: M_∞, β, ϵ_s, δ_{det}, C, and $\frac{x'}{d'} = 0.5C \cot \delta_{det}$.

From reference 9 (see also fig. 9 of this paper) and in terms of the present parameters

$$\frac{y}{d'} = \frac{1}{\beta}\sqrt{\left(\frac{x}{d'}\right)^2 - \left(\frac{x_0}{d'}\right)^2} \tag{C1}$$

Similarly, the results of reference 9 can be used to obtain

$$\frac{x_0}{d'} = \frac{\beta\sqrt{\beta^2\tan^2\epsilon_s - 1}\left(\frac{x'}{d'} + \frac{\tan\eta}{2}\right)}{\beta^2\tan\epsilon_s - \beta\sqrt{\beta^2\tan^2\epsilon_s - 1} + \tan\eta} \tag{C2}$$

Combining equations (C1) and (C2) yields

$$\tan\eta = \frac{\sqrt{\left(\frac{x}{d'}\right)^2 - \left[\beta\left(\frac{y}{d'}\right)\right]^2}\left(\beta^2\tan\epsilon_s - \beta\sqrt{\beta^2\tan^2\epsilon_s - 1}\right) - \frac{x'}{d'}\beta\sqrt{\beta^2\tan^2\epsilon_s - 1}}{\frac{\beta}{2}\sqrt{\beta^2\tan^2\epsilon_s - 1} - \sqrt{\left(\frac{x}{d'}\right)^2 - \left[\beta\left(\frac{y}{d'}\right)\right]^2}} \tag{C3}$$

The quantities y/d' and x/d' are the ordinates of a point on the known shock shape. The shape, however, is usually given or obtained in terms of the maximum diameter D and with distance in the x-direction measured from the center of the spherical (or circular) nose or from the face of a flat nose. This distance will be called F herein. The following simple expressions for obtaining y/d' and x/d' from these dimensions are given for the spherical (or circular) nose:

$$\frac{y}{d'} = \frac{y}{D} \frac{1}{\cos \delta_{det}} \tag{C4}$$

and for the flat nose:

$$\frac{y}{d'} = \frac{y}{D} \tag{C5}$$

Values of x/d' are obtained from

$$\frac{x}{d'} = \frac{\psi^2 + \left[\beta\left(\frac{y}{d'}\right)\right]^2}{2\psi} \tag{C6}$$

where the quantity ψ has the following value for the spherical (or circular) nose:

$$\psi = \frac{1}{\cos \delta_{det}}\left(\frac{F}{D} + \frac{\sin^2\delta_{det} + C \cos^2\delta_{det}}{2 \sin \delta_{det}}\right) \tag{C7}$$

and for the flat nose:

$$\psi = \frac{x'}{d'} - \frac{F}{D} \tag{C8}$$

APPENDIX D

PROCEDURE FOR CALCULATING SHOCK SHAPE

The following quantities are known or can be determined according to the methods suggested in the text: M_∞, β, ϵ_s, C, η, δ_{det}, and $\frac{x'}{d'} = 0.5C \cot \delta_{det}$. The value of $\frac{x_0}{d'}$ is obtained from equation (C2). With the value of $\frac{x_0}{d'}$ thus determined, it is convenient to determine $\frac{x}{d'}$ by assigning positive values to the quantity $\frac{x}{d'} - \frac{x_0}{d'}$ from zero upward. The value of $\frac{y}{d'}$ may be calculated from

$$\frac{y}{d'} = \frac{1}{\beta}\sqrt{\left(\frac{x}{d'}\right)^2 - \left(\frac{x_0}{d'}\right)^2} \qquad \text{(D1)}$$

In terms of the diameter D the ordinates become

$$\frac{y}{D} = \left(\frac{y}{d'}\right)\cos \delta_{det} \qquad \text{(D2)}$$

and

$$\frac{F}{D} = \left(\frac{x}{d'} - \frac{x_0}{d'}\right)\cos \delta_{det} - \frac{\sin^2\delta_{det} + C\cos^2\delta_{det}}{2 \sin \delta_{det}} \qquad \text{(D3)}$$

If the slope of the shock at any point is desired, it may be obtained from the relation

$$\frac{dy}{dx} = \frac{\frac{x}{d'}}{\beta\sqrt{\left(\frac{x}{d'}\right)^2 - \left(\frac{x_0}{d'}\right)^2}} \qquad \text{(D4)}$$

REFERENCES

1. Crocco, Luigi: Singolarità della corrente gassosa iperacustica nell'intorno di una prora a diedro. L'Aerotecnica, vol. XVII, fasc. 6, June 1937, pp. 519-534.

2. Frankl, F.: On the Problems of Chaplygin for Mixed Sub- and Supersonic Flows. NACA TM 1155, 1947.

3. Maccoll, J. W.: Investigation of Compressible Flow at Sonic Speeds. Theoretical Res. Rep. No. 7/46, Armament Res. Dept., British Ministry of Supply, Sept. 1946.

4. Guderley, K. Gottfried: Considerations of the Structure of Mixed Subsonic-Supersonic Flow Patterns. Tech. Rep. No. F-TR-2168-ND, Air Materiel Command, U. S. Air Force, Oct. 1947.

5. Busemann, Adolf: A Review of Analytical Methods for the Treatment of Flows With Detached Shocks. NACA TN 1858, 1949.

6. Maccoll, J. W., and Codd, J.: Theoretical Investigations of the Flow Around Various Bodies in the Sonic Region of Velocities. British Theoretical Res. Rep. No. 17/45, B. A. R. C. 45/19, British Ministry of Supply, Armament Res. Dept., 1945.

7. Liepmann, Hans Wolfgang, Askenas, Harry, and Cole, Julian D.: Experiments in Transonic Flow. AF Tech. Rep. No. 5667, Air Materiel Command, Feb. 9, 1948. (Prepared by C. I. T., June 1947, under AAF Contract No. W33-038ac-1717 (11592).)

8. Laitone, Edmund V., and Pardee, Otway O'M.: Location of Detached Shock Wave in Front of a Body Moving at Supersonic Speeds. NACA RM A7B10, 1947.

9. Moeckel, W. E.: Approximate Method for Predicting Form and Location of Detached Shock Waves Ahead of Plane or Axially Symmetric Bodies. NACA TN 1921, 1949.

10. Heberle, Juergen W., Wood, George P., and Gooderum, Paul B.: Data on Shape and Location of Detached Shock Waves on Cones and Spheres. NACA TN 2000, 1950.

11. Moeckel, W. E.: Experimental Investigation of Supersonic Flow With Detached Shock Waves for Mach Numbers Between 1.8 and 2.9. NACA RM E50D05, 1950.

12. Guderley, K. Gottfried: Singularities at the Sonic Velocity (Project No. HA-219). Tech. Rep. No. F-TR-1171-ND, ATI No. 23965, Air Materiel Command, U. S. Air Force, June 1948.

13. Vincenti, Walter G., and Wagoner, Cleo B.: Transonic Flow Past a Wedge Profile With Detached Bow Wave. NACA Rep. 1095, 1952. (Supersedes NACA TN's 2339 and 2588.)

14. Yoshihara, Hideo: On the Flow Over a Finite Wedge in the Lower Transonic Region. WADC Tech. Rep. 56-444, Wright Air Dev. Center, U. S. Air Force, June 1956. (Available as ASTIA Doc. No. AD 110428.)

15. Hida, Kinzo: An Approximate Study on the Detached Shock Wave in Front of a Circular Cylinder and a Sphere. Jour. Phys. Soc. of Japan, vol. 8, no. 6, Nov.-Dec. 1953, pp. 740-745.

16. Serbin, H.: Hypersonic, Non-Viscous Flow Around a Circular Disk Normal to the Stream. U. S. Air Force Project RAND Res. Memo. RM-1713, The RAND Corp., May 3, 1956.

17. Drougge, George.: The Flow Around Conical Tips in the Upper Transonic Range. Rep. No. 25, Aero. Res. Inst. of Sweden (Stockholm), 1948.

18. Li, Ting-Yi, and Geiger, Richard E.: Stagnation Point of a Blunt Body in Hypersonic Flow. Jour. Aero. Sci., vol. 24, no. 1, Jan. 1957, pp. 25-32.

19. Heybey, W. H.: Shock Distances in Front of Symmetrical Bodies. NAVORD Rep. 3594, U. S. Naval Ord. Lab (White Oak, Md.), Dec. 24, 1953.

20. Oliver, Robert E.: An Experimental Investigation of Flow Over Simple Blunt Bodies at a Nominal Mach Number of 5.8. GALCIT Memo. No. 26 (Contract No. DA-04-495-Ord-19), June 1, 1955.

21. Hayes, Wallace D.: Some Aspects of Hypersonic Flow. The Ramo-Wooldridge Corp., Jan. 4, 1955.

22. Lees, Lester, and Kubota, Toshi: Inviscid Hypersonic Flow Over Blunt-Nosed Slender Bodies. Jour. Aero. Sci., vol. 24, no. 3, Mar. 1957, pp. 195-202.

23. Maslen, Stephen H., and Moeckel, W. E.: Inviscid Hypersonic Flow Past Blunt Bodies. Preprint No. 665, S.M.F. Fund Preprint, Inst. Aero. Sci., Jan. 1957.

24. Kim, Chul-Soo: Experimental Studies of Supersonic Flow Past a Circular Cylinder. Jour. Phys. Soc. of Japan, vol. 11, no. 4, Apr. 1956, pp. 439-445.

25. Alperin, Morton: Experimental Information on Two-Dimensional Detached Shock Waves. Progress Rep. No. 4-44 (ORDCIT Proj. Contract No. W-04-200-ORD-455), C.I.T., Jet Propulsion Lab., May 31, 1950.

26. Uchida, Shigeo, and Yasuhara, Michiru: The Rotational Field Behind a Curved Shock Wave Calculated by the Method of Flux Analysis. Jour. Aero. Sci., vol. 23, no. 9, Sept. 1956, pp. 830-845.

27. Johnston, G. W.: An Investigation of the Flow About Cones and Wedges at and Beyond the Critical Angle. UTIA Rep. No. 24, Inst. Aerophysics, Univ. Toronto, Dec. 1952.

28. Griffith, Wayland C.: Transonic Flow. Tech. Rep. II - 7, Princeton Univ., Dept. of Phys., Dec. 19, 1950.

29. Giese, J. H., and Bergdolt, V. E.: Interferometric Studies of Supersonic Flows About Truncated Cones. Jour. Appl. Physics, vol. 24, no. 11, Nov. 1953, pp. 1389-1396.

30. Charters, A. C., and Stein, H.: The Drag of Projectiles With Truncated Cone Headshapes. Rep. No. 624, Ballistic Res. Labs., Aberdeen Proving Ground, Mar. 1952.

31. Chester, W.: Supersonic Flow Past a Bluff Body With a Detached Shock. Part I. Two-Dimensional Body. Jour. Fluid Mech., vol. 1, pt. 4, Oct. 1956, pp. 353-365.

32. Freemän, N. C.: On the Theory of Hypersonic Flow Past Plane and Axially Symmetric Bluff Bodies. Jour. Fluid Mech., vol. 1, pt. 4, Oct. 1956, pp. 366-387.

33. Bertram, Mitchel H.: Tip-Bluntness Effects on Cone Pressures at M = 6.85. Jour. Aero. Sci. (Readers' Forum), vol. 23, no. 9, Sept. 1956, pp. 898-900.

34. Bennett, F. D.: Note on Tip-Bluntness Effects in the Supersonic and Hypersonic Regimes. Jour. Aero. Sci. (Readers' Forum), vol. 24, no. 4, Apr. 1957, pp. 314-315.

35. Maccoll, J. W.: The Conical Shock Wave Formed by a Cone Moving at High Speed. Proc. Roy. Soc. (London), ser. A, vol. 159, no. 898, Apr. 1, 1937, pp. 459-472.

36. Serbin, H.: Hypersonic, Non-Viscous Flow Around a Sphere. U. S. Air Force Project RAND Res. Memo. RM-1772, The RAND Corp., Aug. 13, 1956.

37. Ames Research Staff: Equations, Tables, and Charts for Compressible Flow. NACA Rep. 1135, 1953. (Supersedes NACA TN 1428.)

38. Crawford, Davis H., and McCauley, William D.: Investigation of the Laminar Aerodynamic Heat-Transfer Characteristics of a Hemisphere-Cylinder in the Langley 11-Inch Hypersonic Tunnel at a Mach Number of 6.8. NACA TN 3706, 1956.

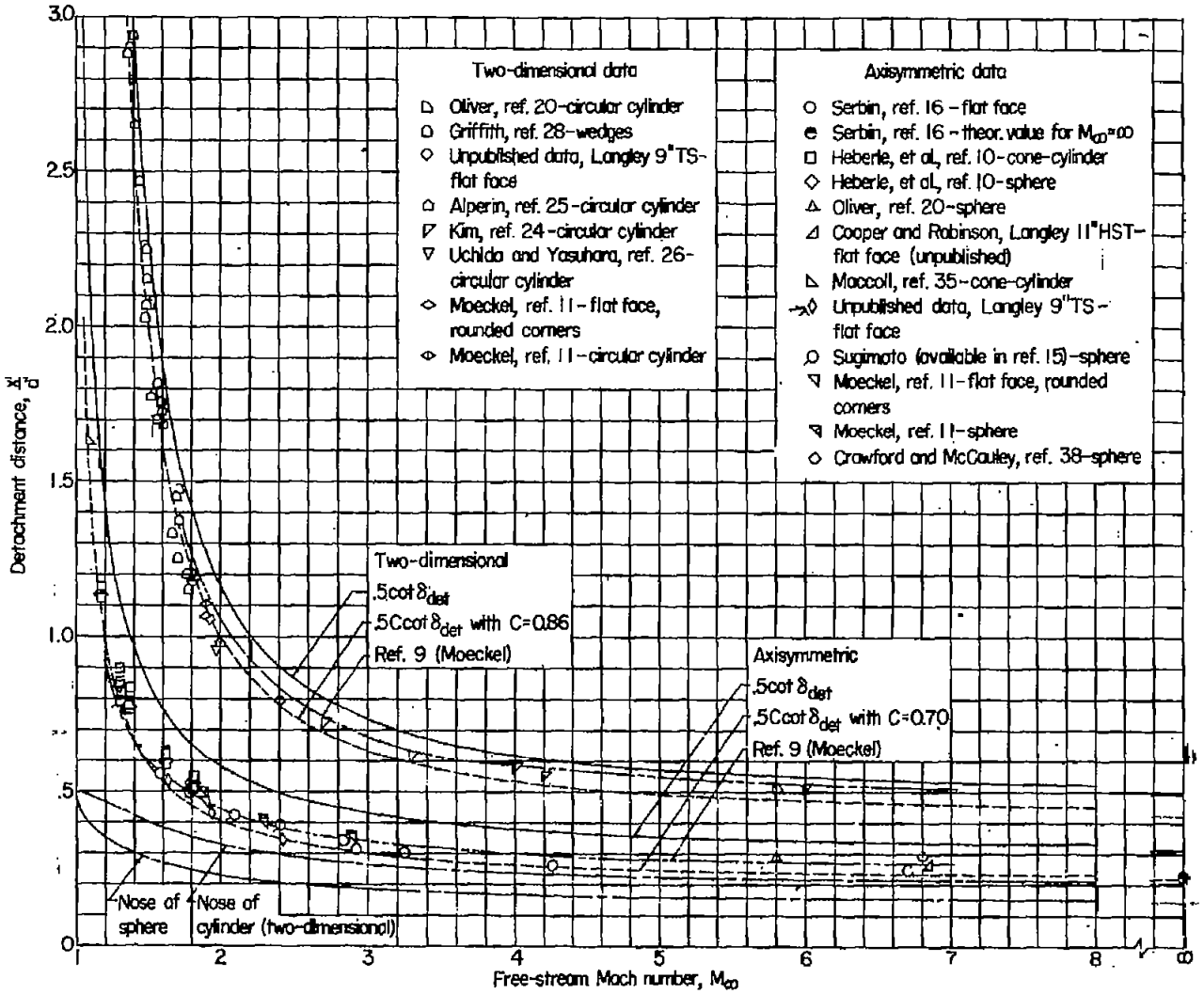

Figure 1.- Compilation and general correlation of data on detachment distance for two-dimensional and axisymmetric nose shapes in air. $\gamma = 1.4$.

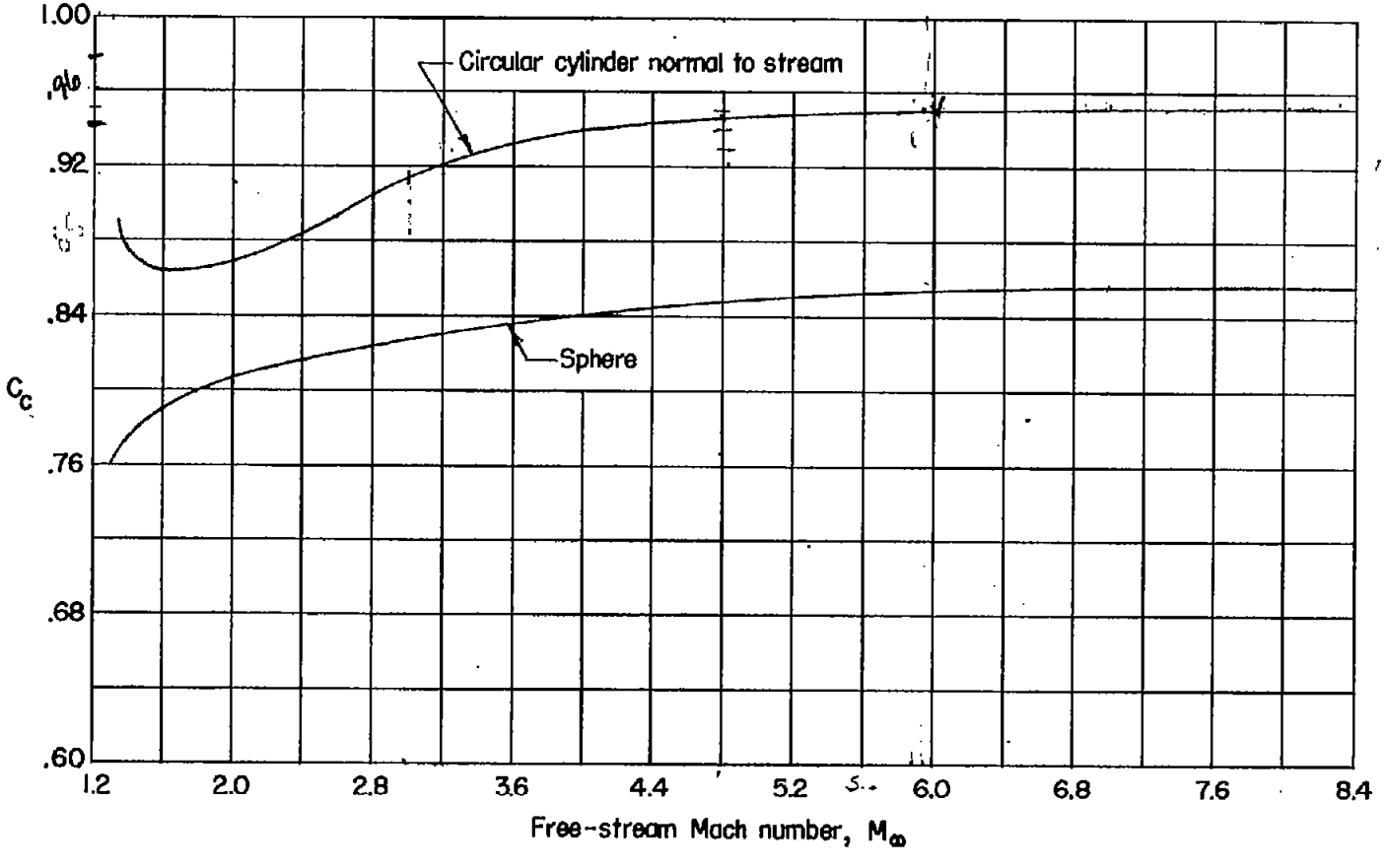

Figure 2.- Variation of C_c with Mach number.

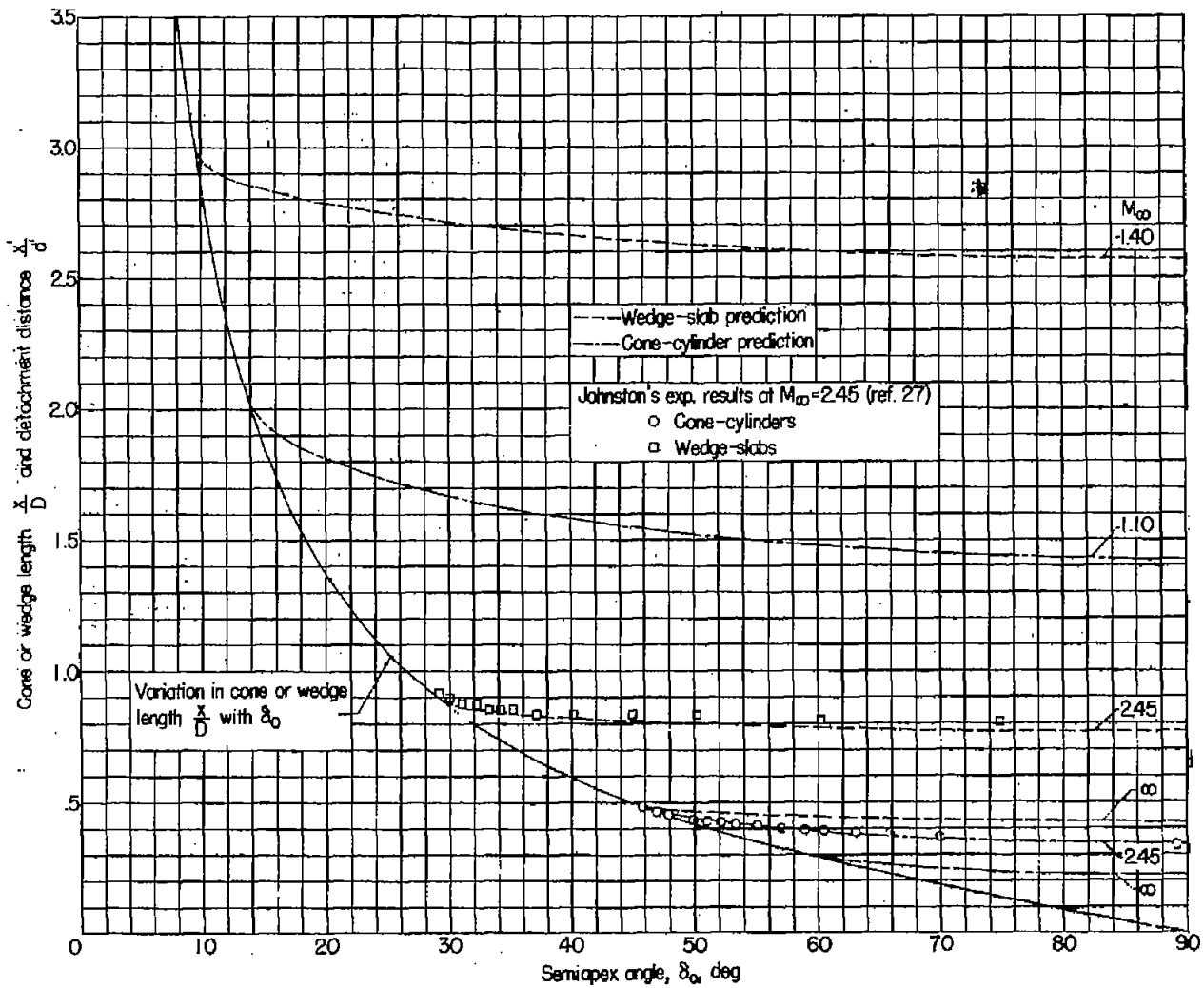

Figure 3.- Variation in detachment distance with semiapex angle for cone-cylinders and wedge-slabs at constant Mach number.

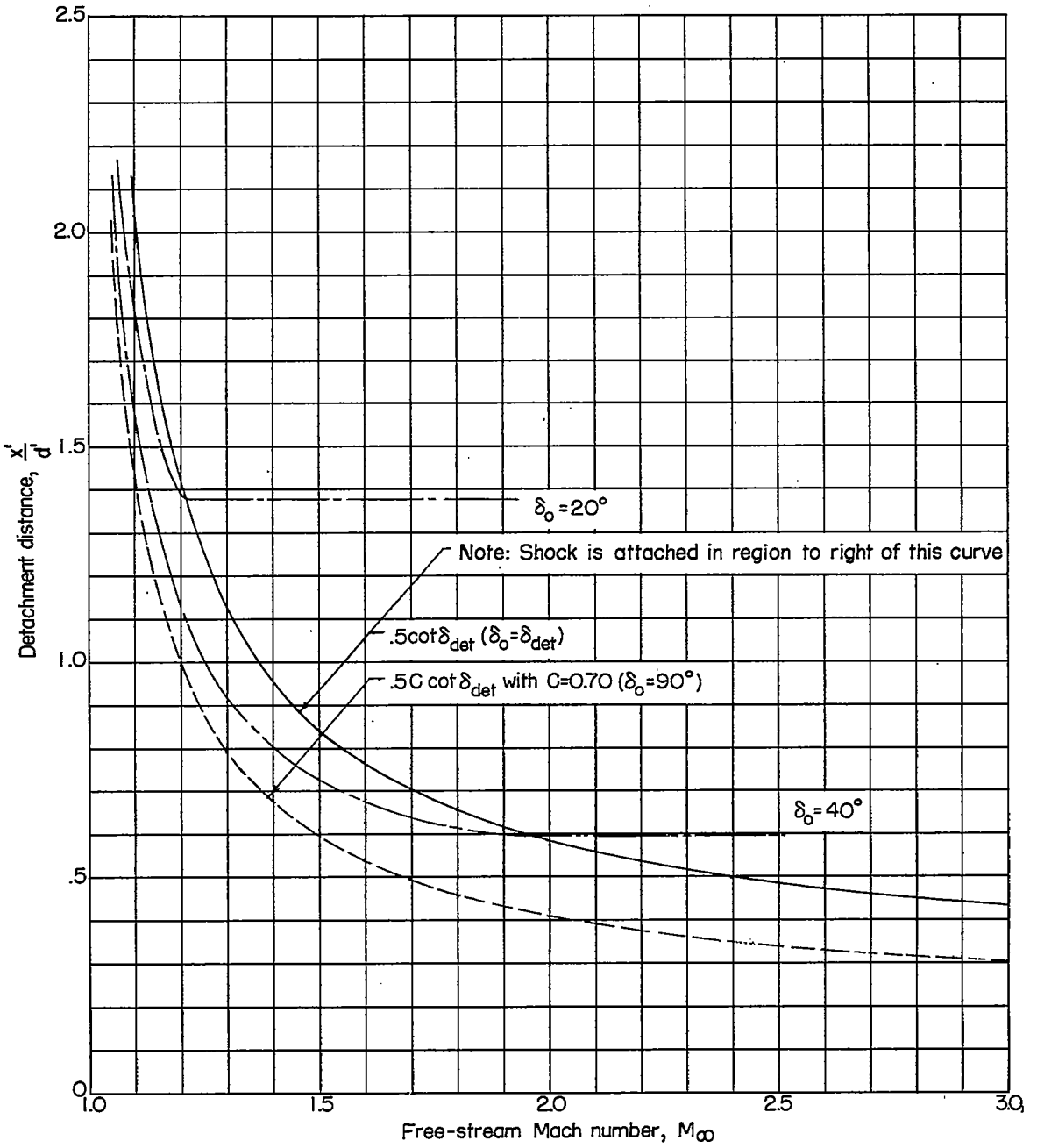

Figure 4.- Predicted variation in detachment distance with Mach number for cone-cylinders at constant semiapex angle.

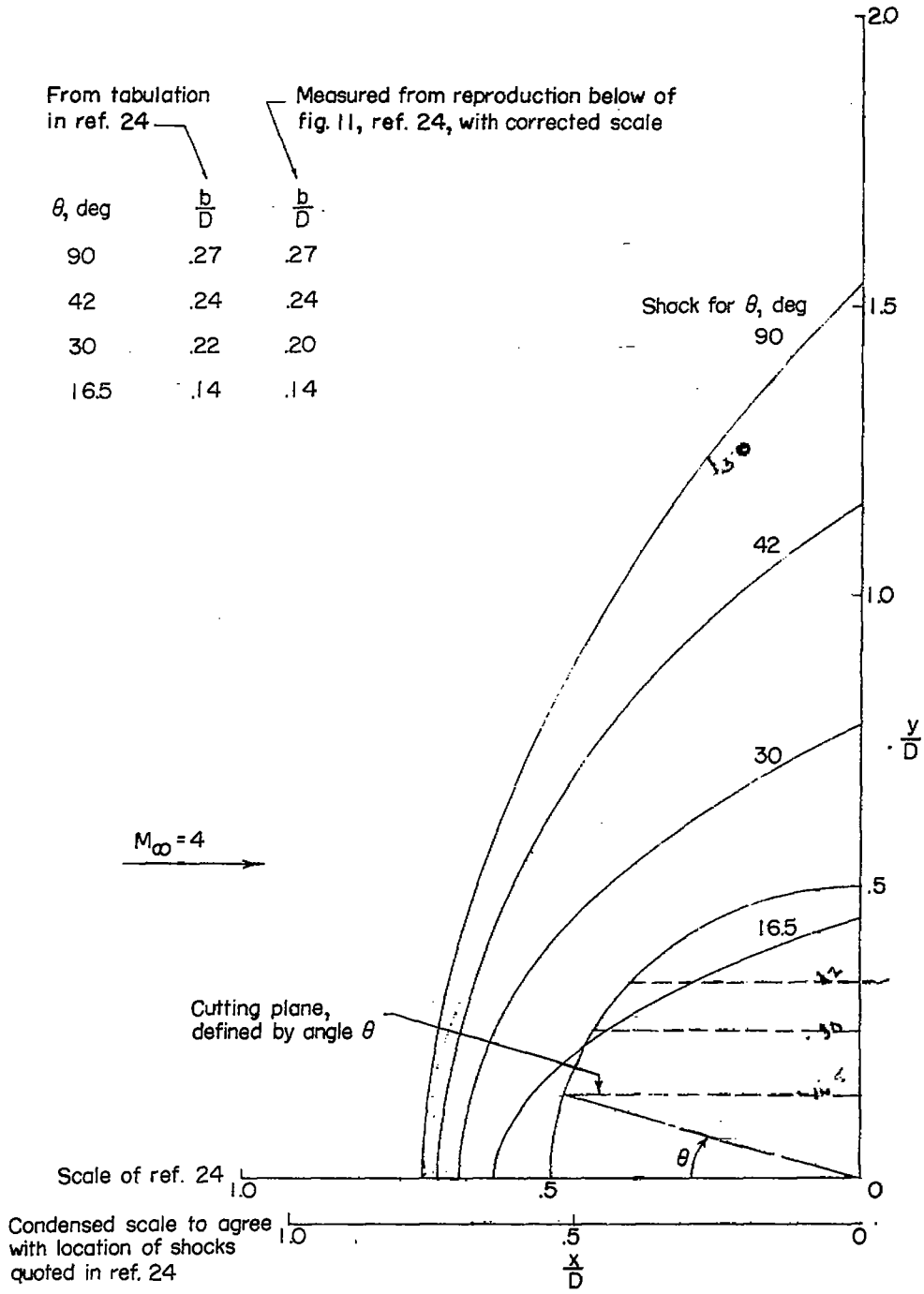

Figure 5.- Reproduction of shock shapes reported by Kim in reference 24.

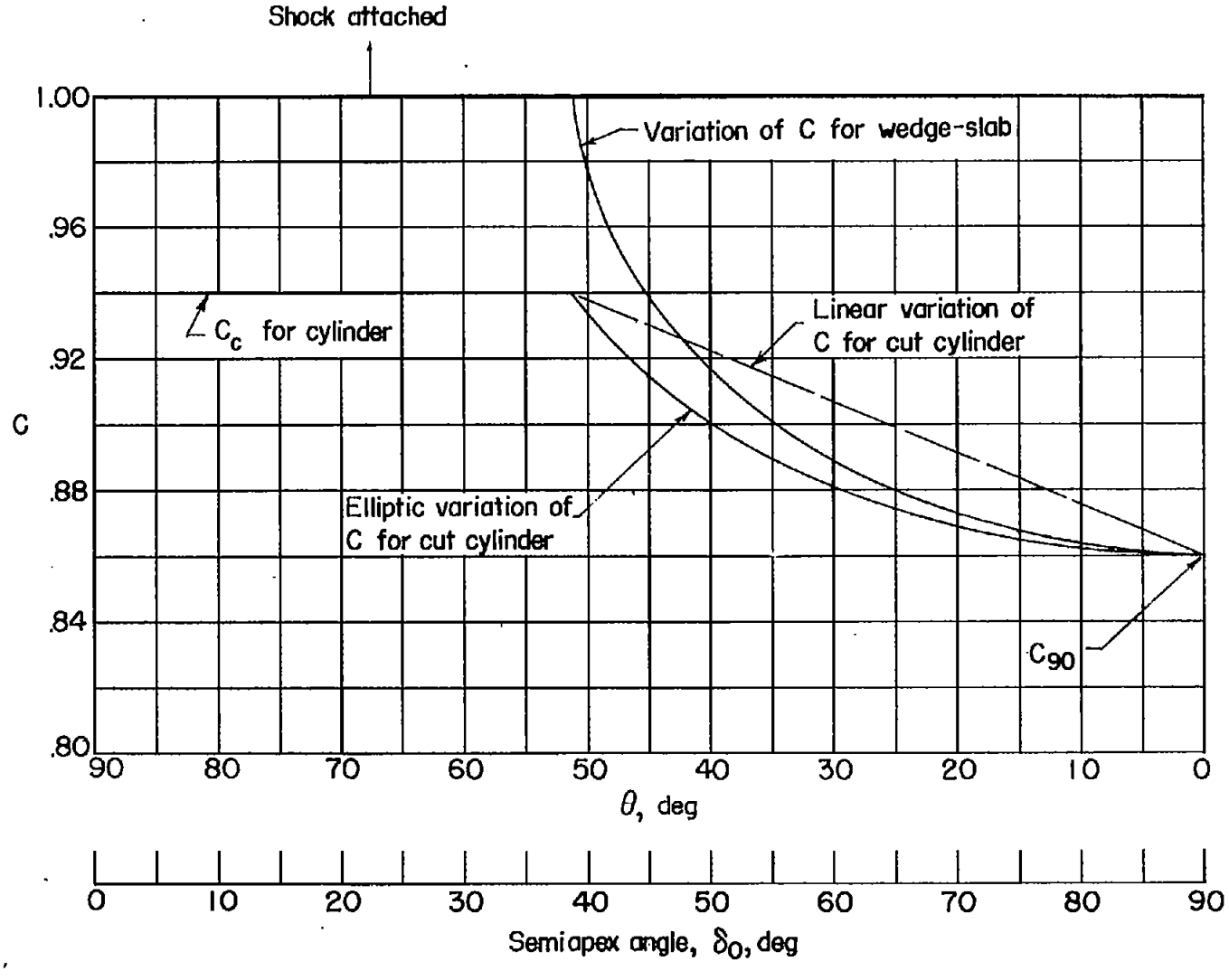

Figure 6.- Calculated linear and elliptic variation of C for cut circular cylinder (two-dimensional) at $M_\infty = 4$.

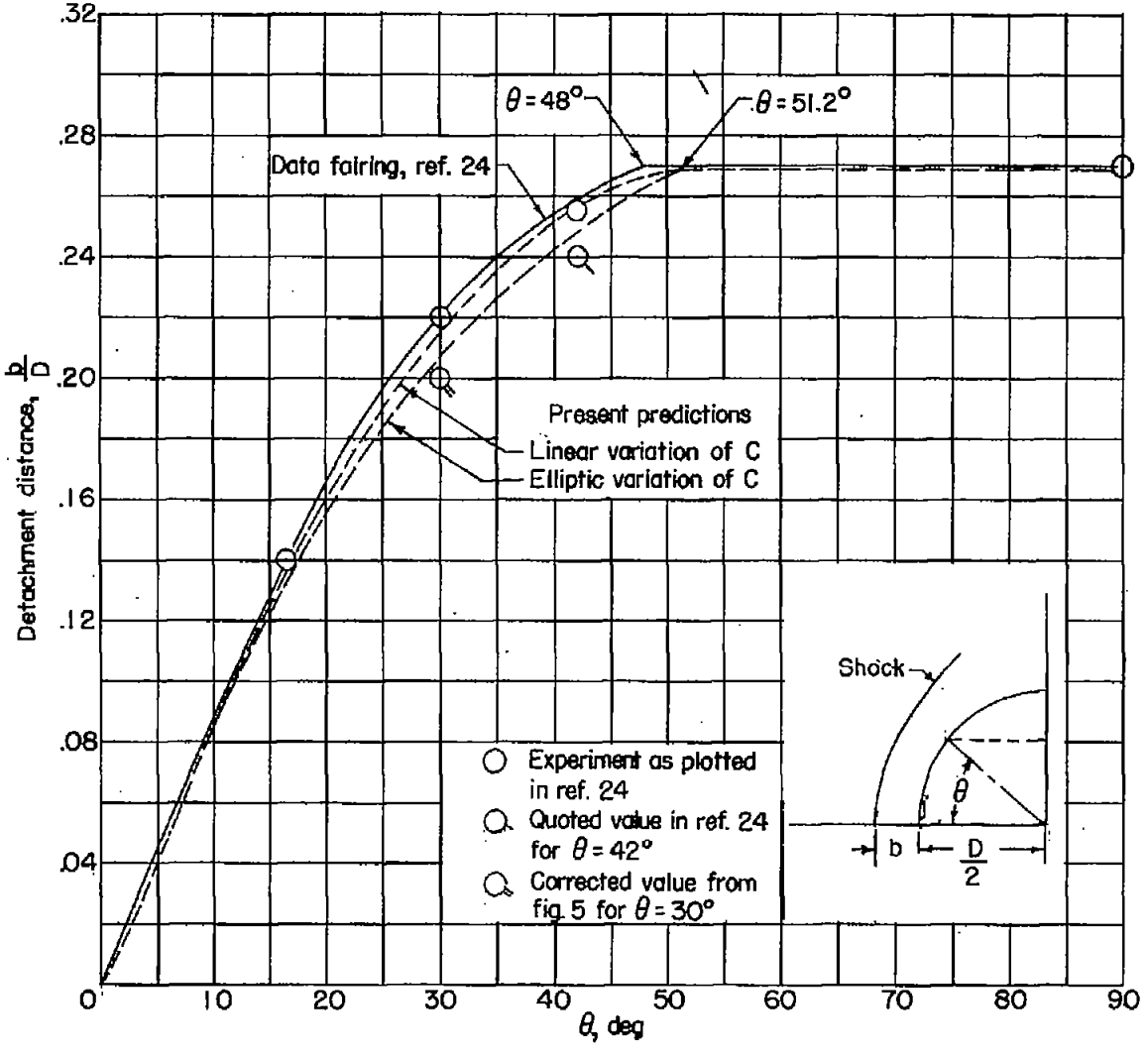

Figure 7.- Prediction of Kim's results (ref. 24) for cut circular cylinder (two-dimensional) at $M_\infty = 4$.

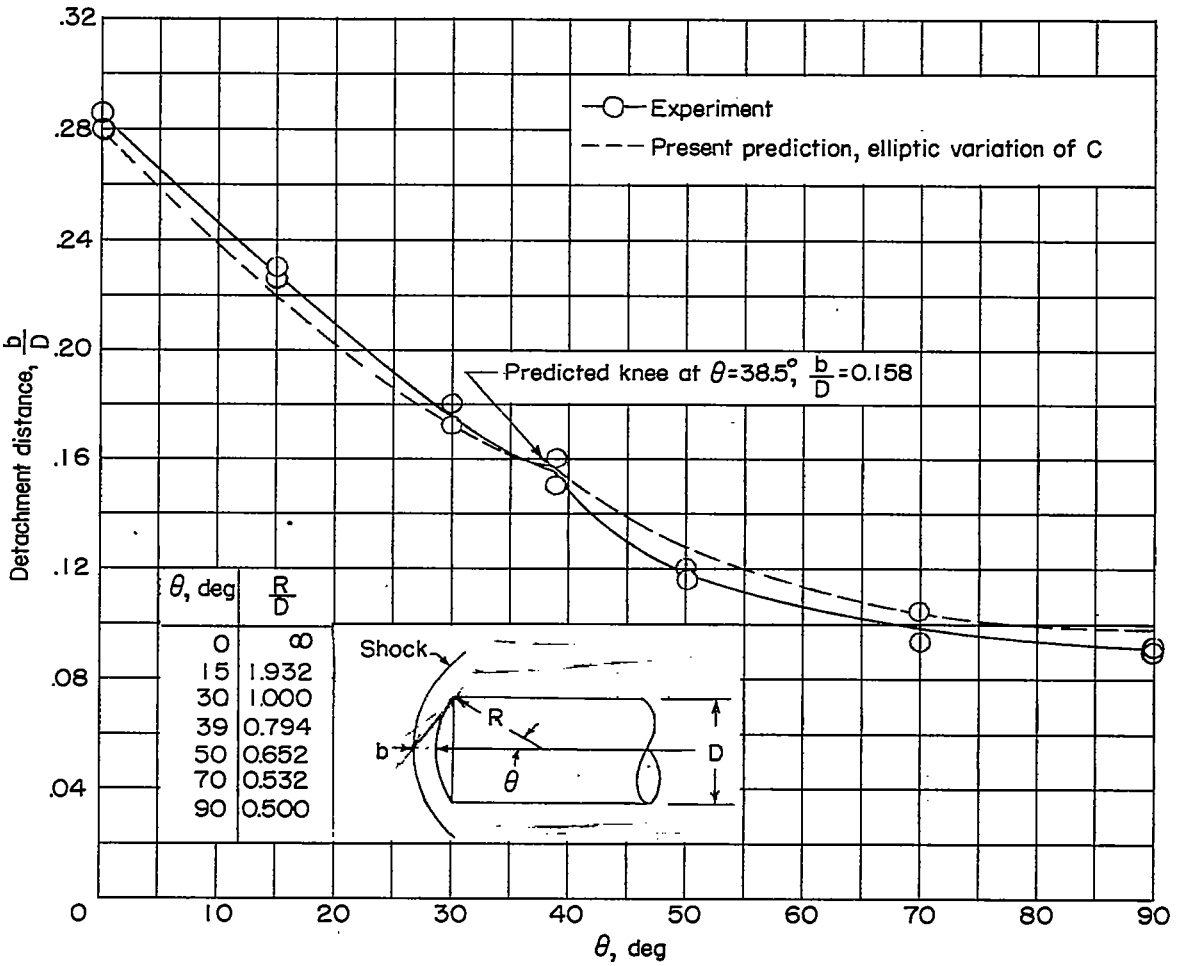

Figure 8.- Prediction of results at $M_\infty = 3.55$ for a sphere that is effectively cut. (Diameter of actual models held constant and radius of nose varied.)

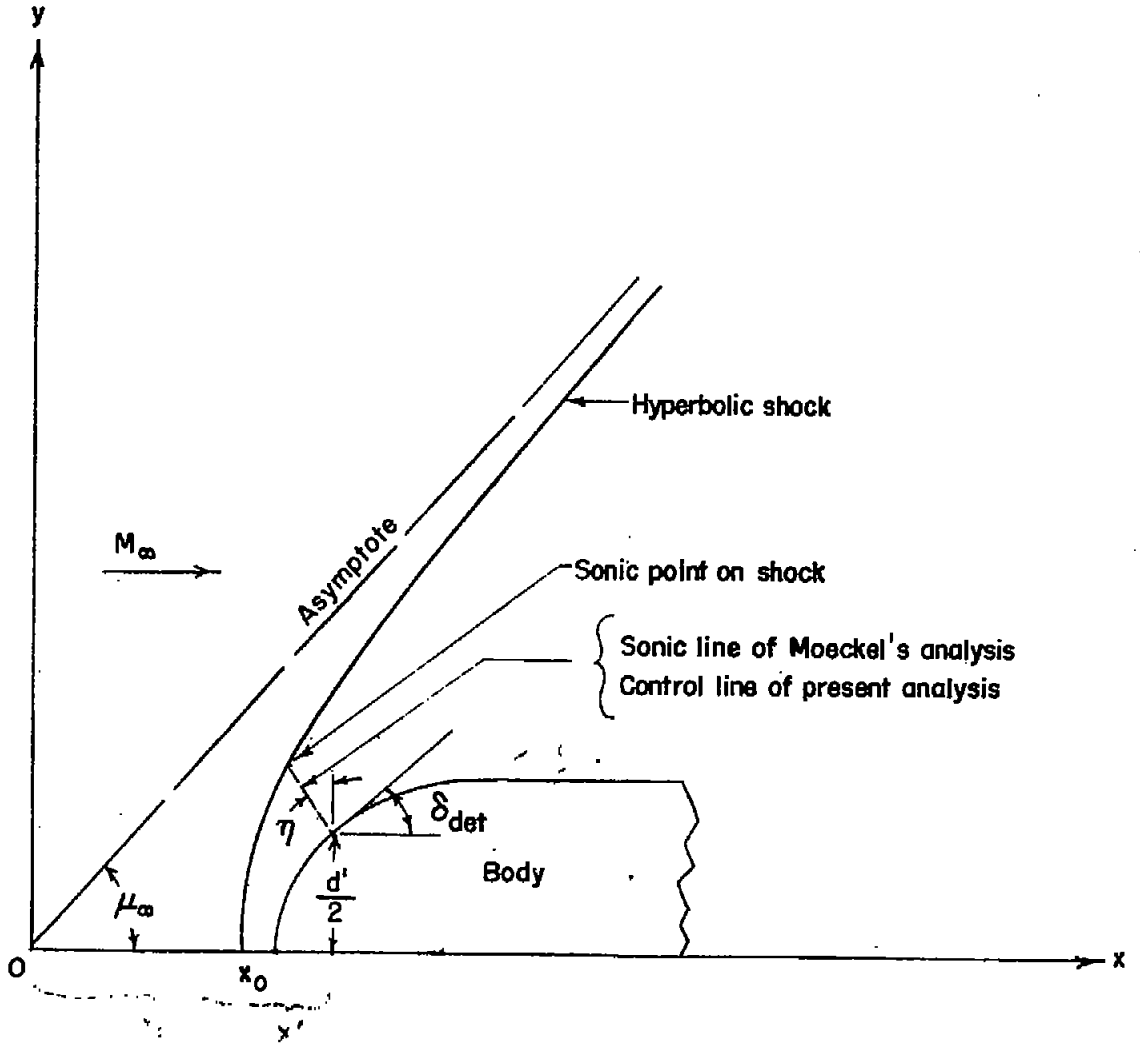

Figure 9.- General features of the method of Moeckel (ref. 9) adopted in present analysis.

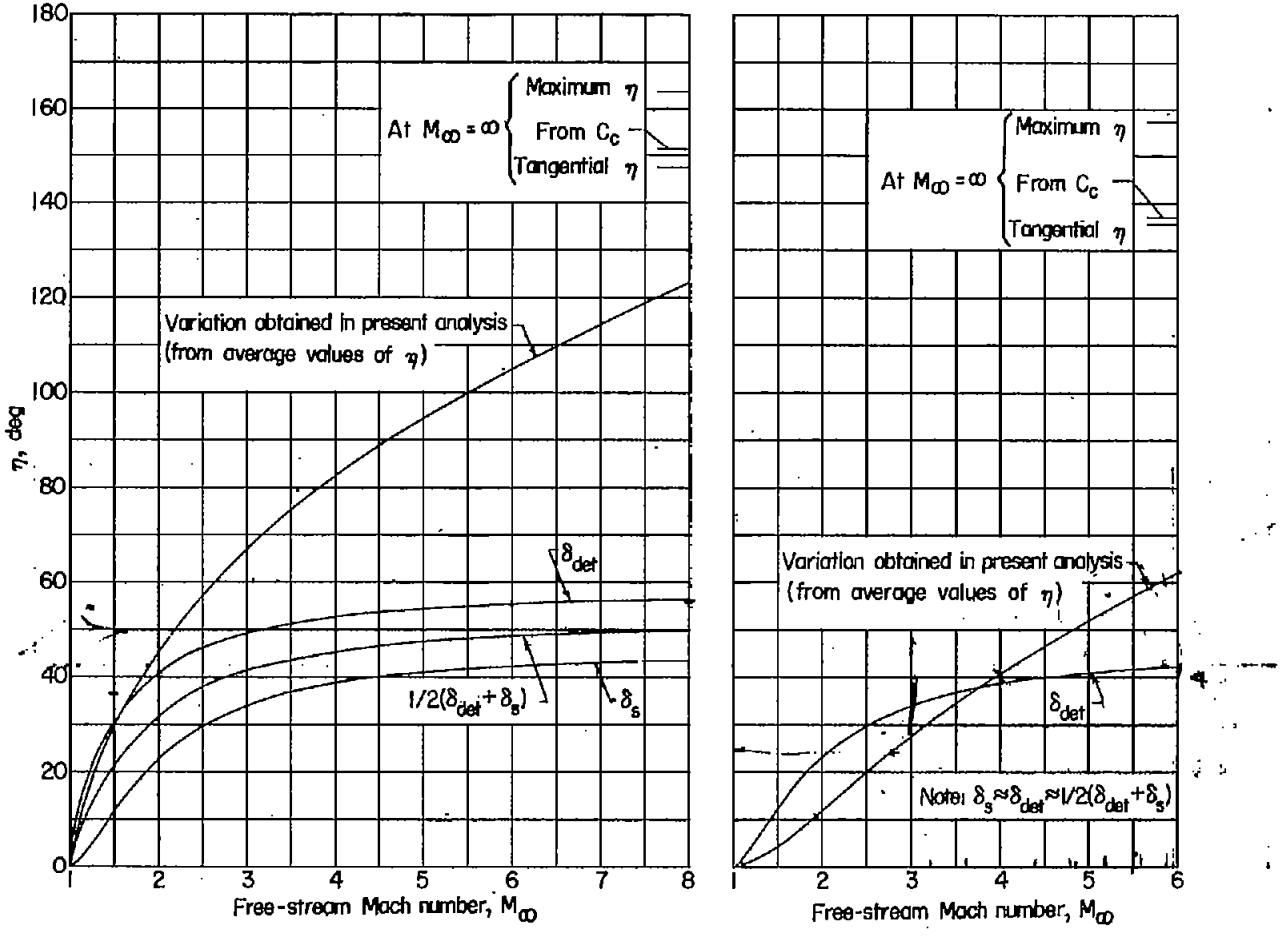

(a) Sphere. (b) Circular cylinder (two-dimensional).

Figure 10.- Comparison of variation of η with Mach number obtained in present analysis with those obtained in other analyses.

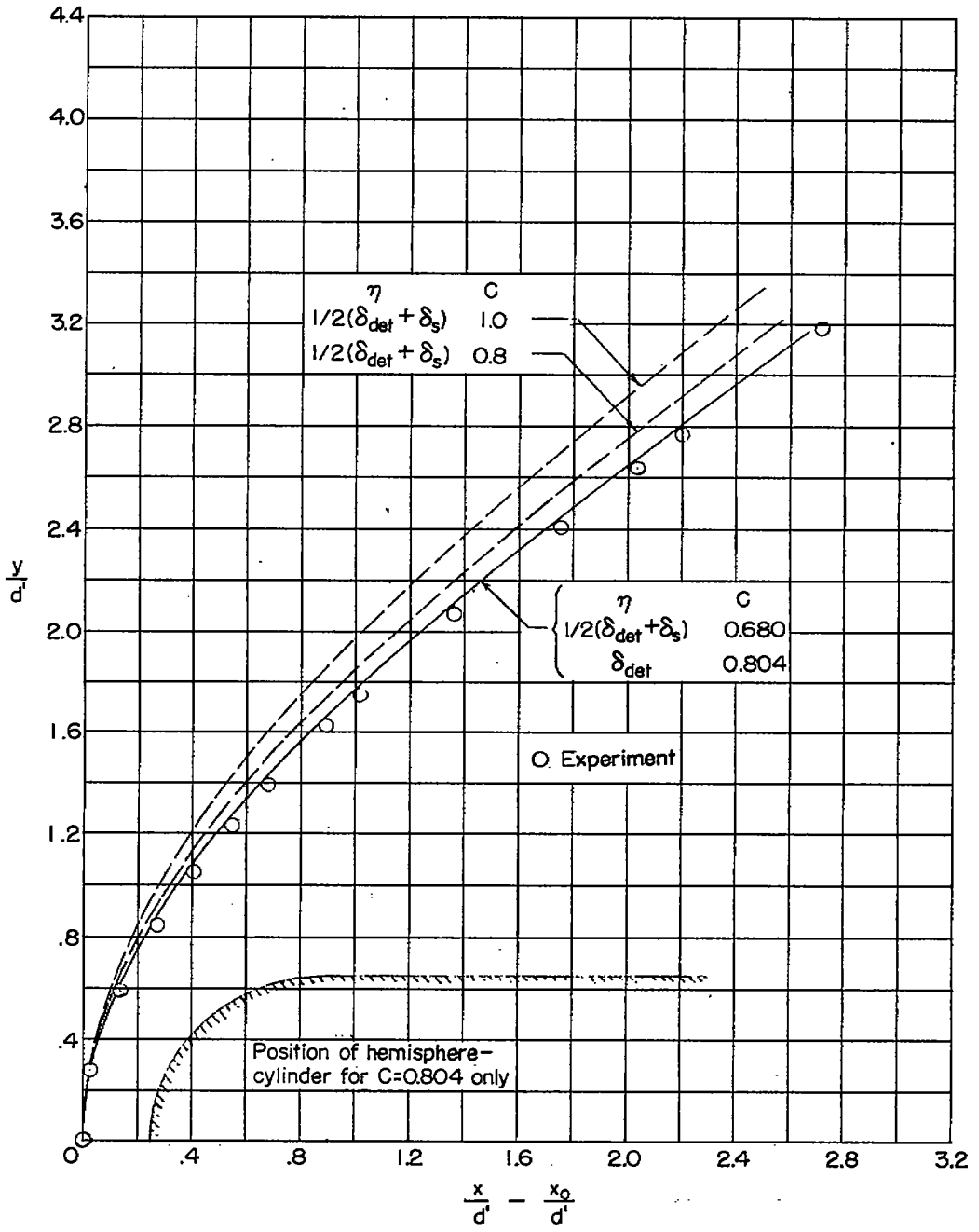

Figure 11.- Effect of C upon shock shape and the possible ambiguity that can occur with the present analysis when the shock is presented in this form. $M_\infty = 1.94$.

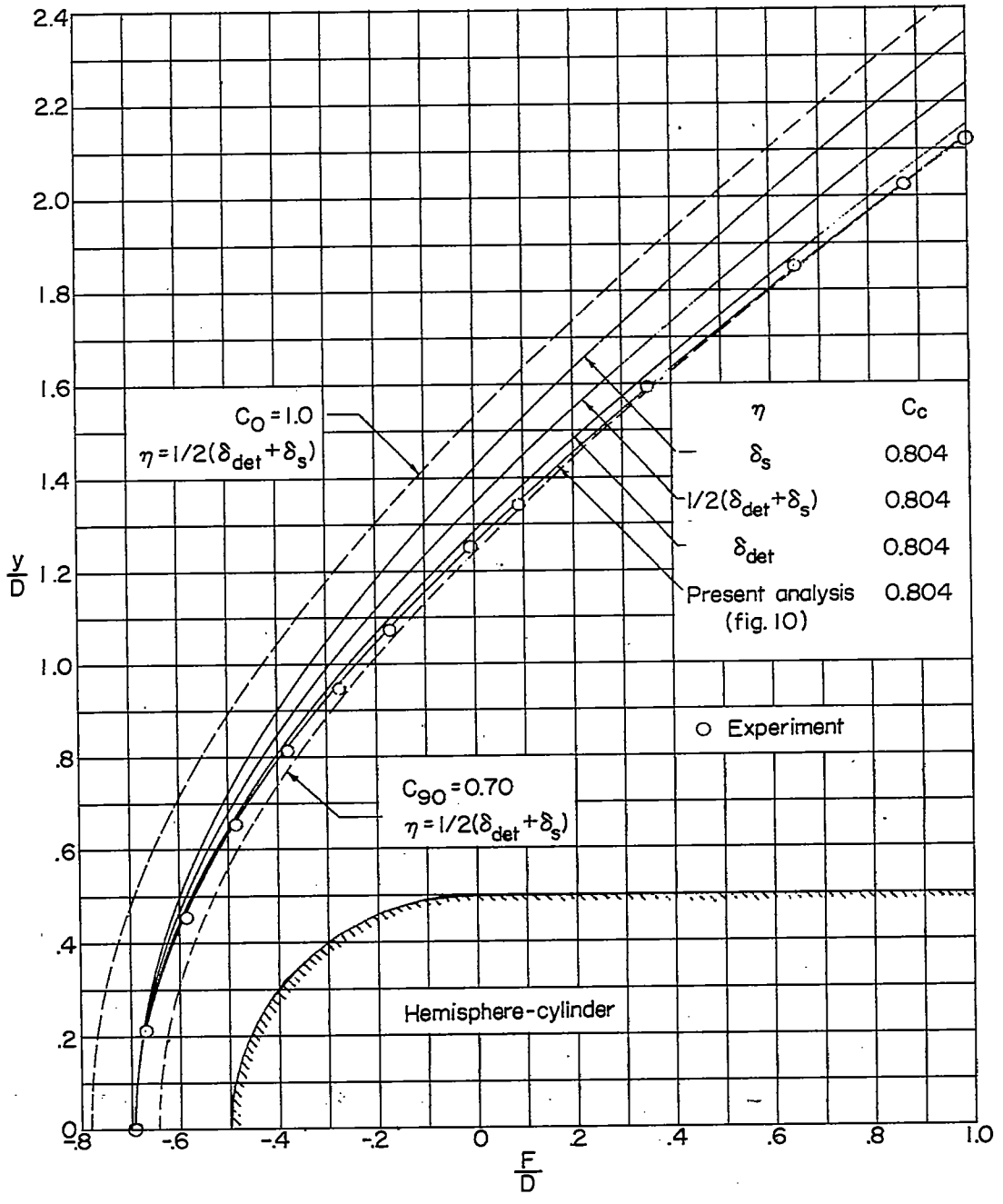

Figure 12.- Effect of η upon shock shape and the effects of C_c upon shock shape within the C-limits of the present analysis for $\eta = 1/2(\delta_{det} + \delta_s)$. $M_\infty = 1.94$.

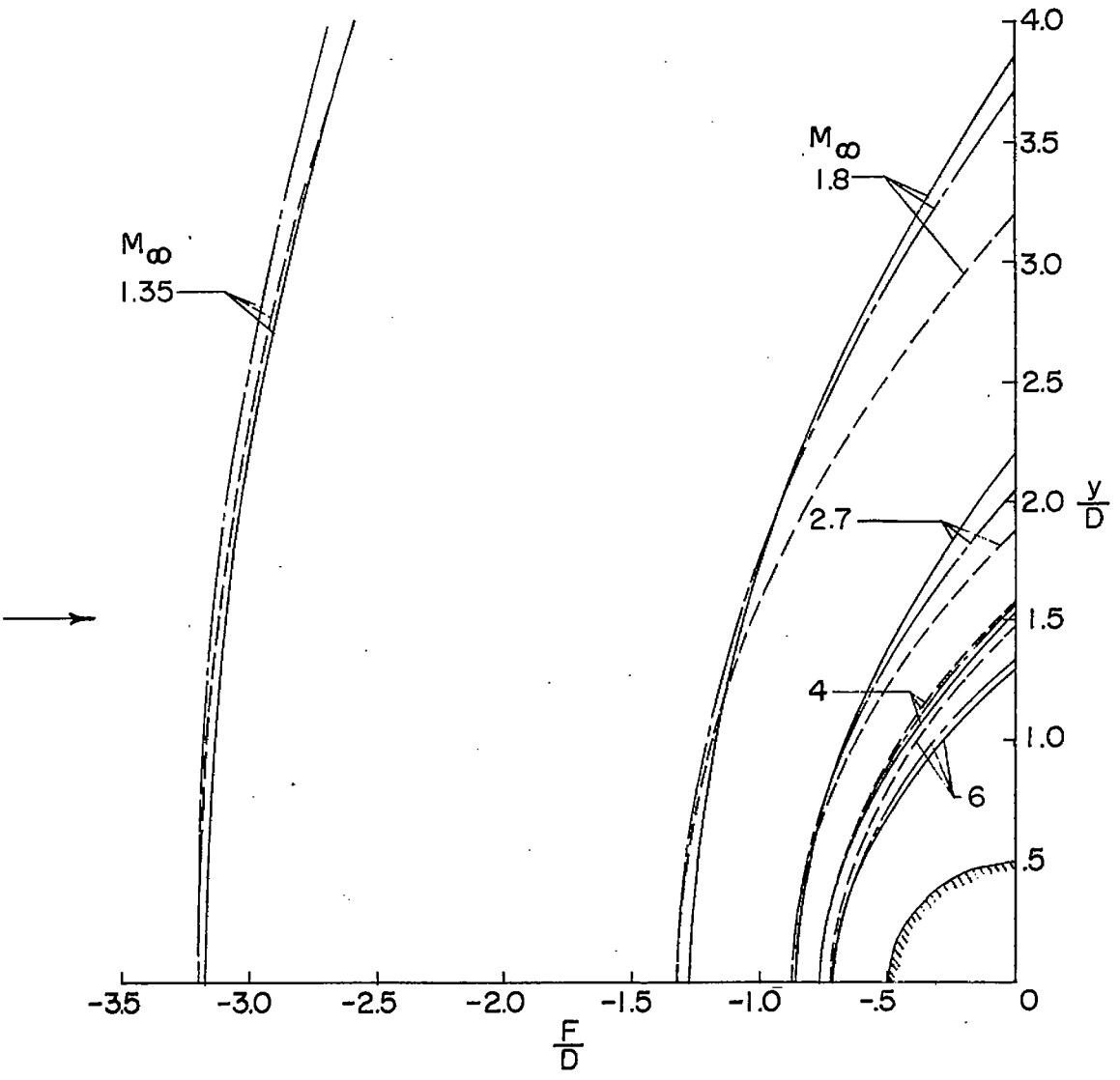

Figure 13.- Prediction of shock shape and location with varying Mach number for a circular cylinder (two-dimensional).

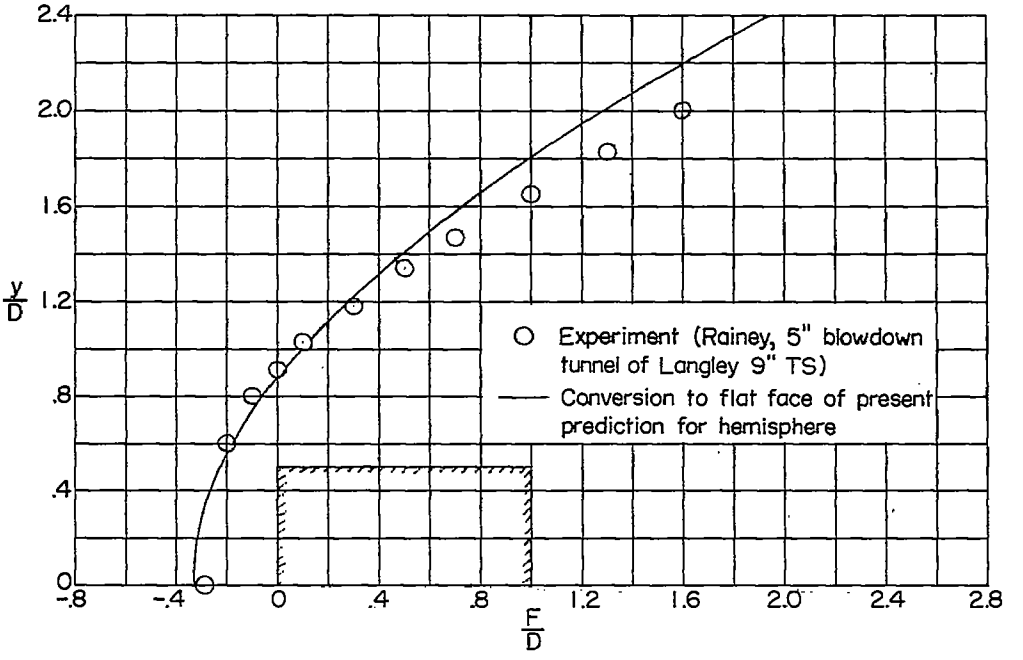

(a) Flat nose.

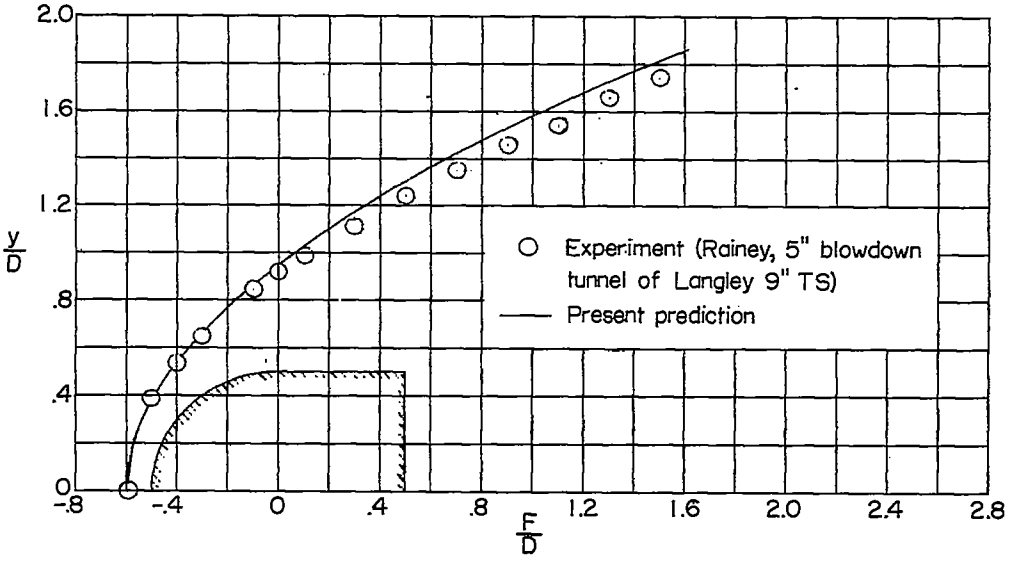

(b) Hemispherical nose.

Figure 14.- Prediction of shock shape and location for axisymmetric noses at $M_\infty = 3.55$.

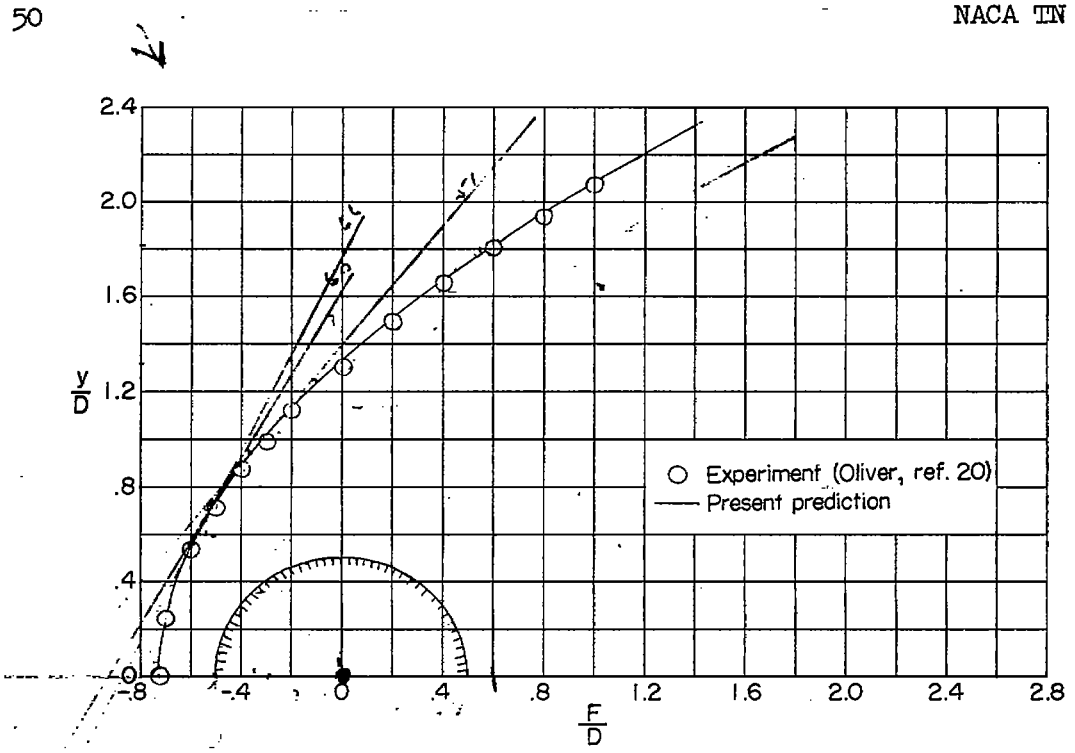

(a) Circular cylinder.

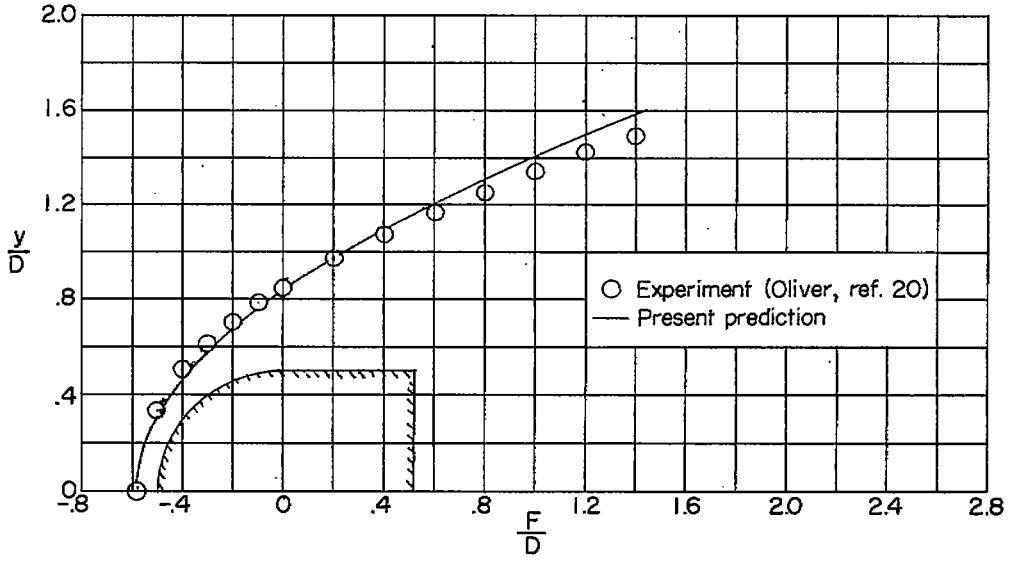

(b) Hemispherical nose.

Figure 15.- Prediction of shock shape and location for hemisphere and circular cylinder (two-dimensional) at $M_\infty = 5.8$.

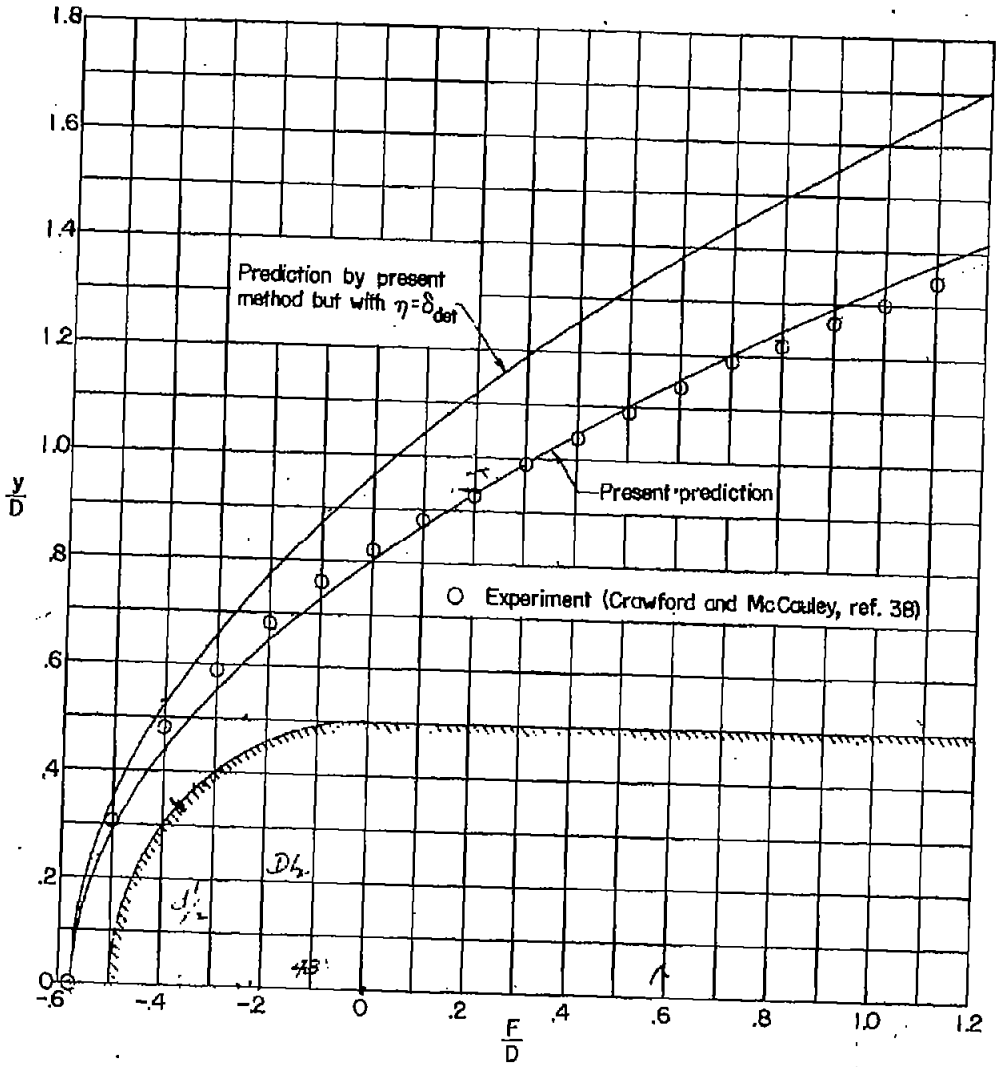

(a) Hemispherical nose.

Figure 16.- Prediction of shock shape and location for axisymmetric noses at $M_\infty = 6.8$.

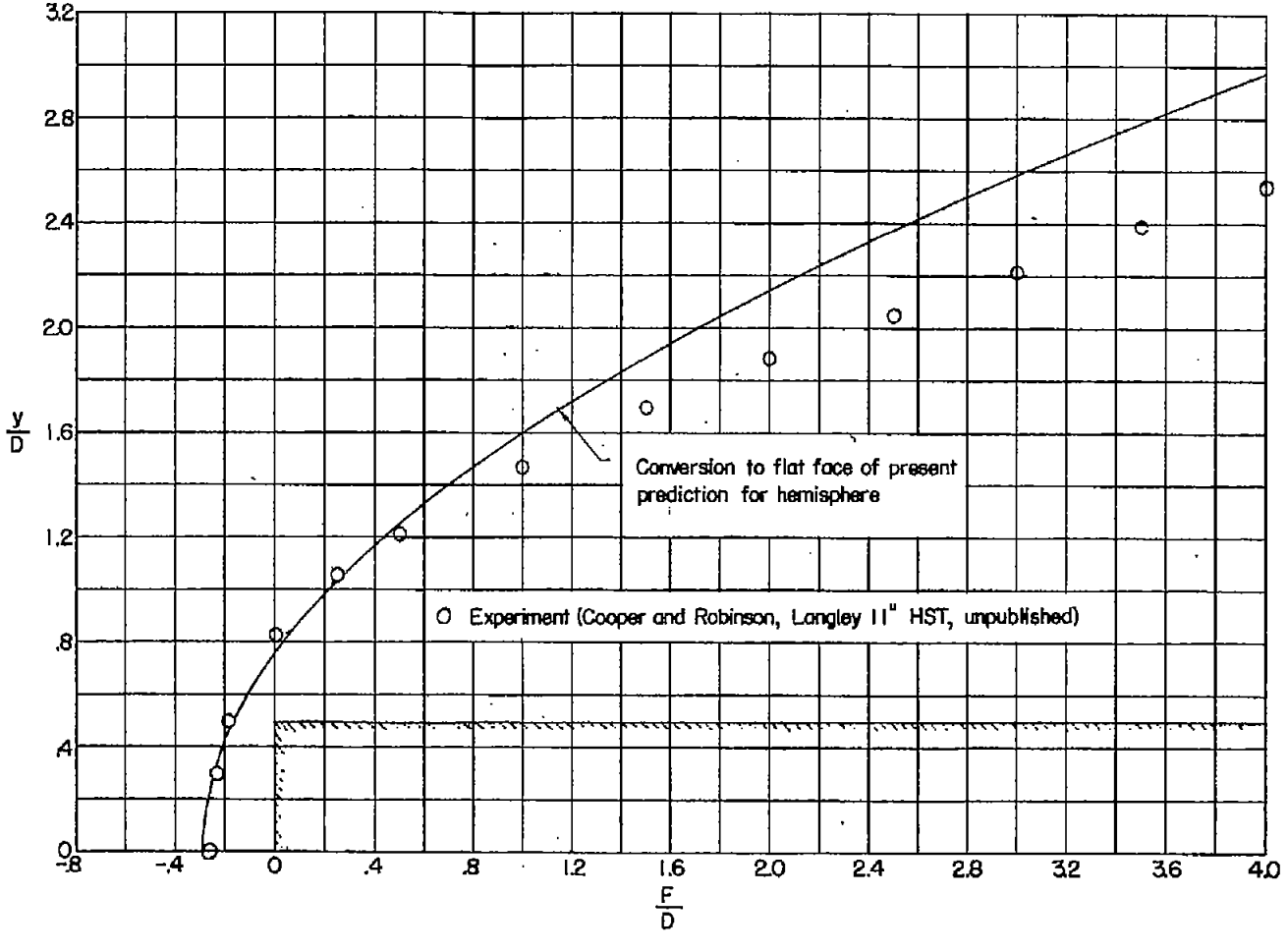

(b) Flat nose.

Figure 16.- Concluded.

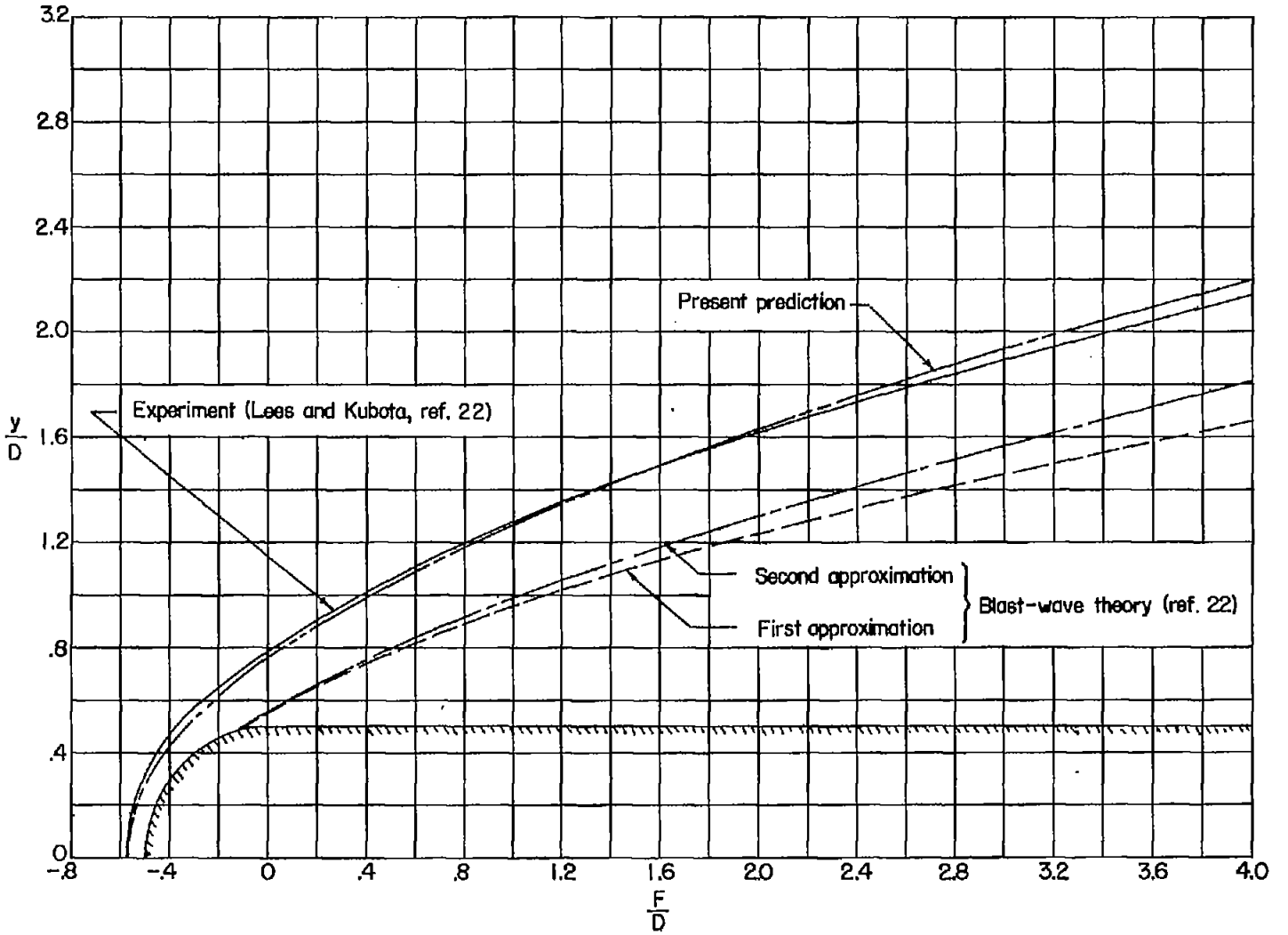

Figure 17.- Prediction of shock shape and location for hemisphere-cylinder at $M_\infty = 7.7$.